Max-Planck-Institut
für Meteorologie

REPORT No. 291

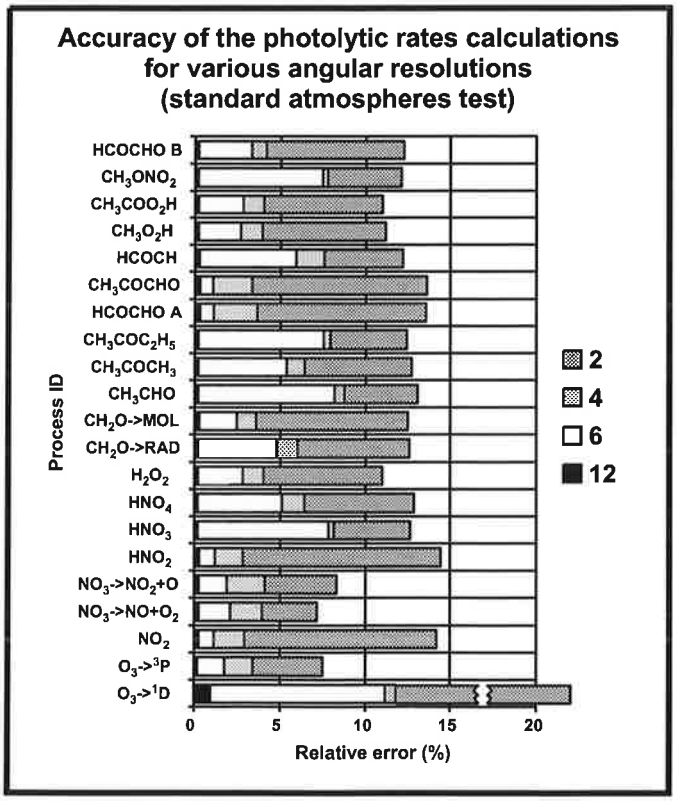

RAPID ALGORITHMS FOR PLANE-PARALLEL RADIATIVE TRANSFER CALCULATIONS

by

Vassili Prigarin

HAMBURG, June 1999

AUTHOR:

Vassili Prigarin

Max-Planck-Institut
für Meteorologie

Computers Center of the Academy of Sciences
of the Russian Federation
Vavilova st. 40, 117333 Moscow
Russia

MAX-PLANCK-INSTITUT
FÜR METEOROLOGIE
BUNDESSTRASSE 55
D - 20146 HAMBURG
GERMANY

Tel.: +49-(0)40-4 11 73-0
Telefax: +49-(0)40-4 11 73-298
E-Mail: <name> @ dkrz.de

Rapid algorithms for plane-parallel radiative transfer calculations

Vassili Prigarin

Computers Center of the Academy of Sciences of the Russian Federation
Vavilova st. 40, 117333 Moscow, Russia

June 1999

ISSN 0937-1060

Abstract - Finite-difference approximations to the radiative transfer equation are presented and the solution procedures for plane-parallel fluxes and intensities computations are discussed. It is shown that, while maintainig the same level of accuracy, the proposed algorithms are up to several hundred times faster than other established solvers. Data sources and physical parameterisations are discussed further and the application of the developed software to the calculation of the photolytic rates is presented. Uncertainties and sources of errors are analysed in the concluding sections.

1. Introduction

Plane-parallel radiative transfer computations are a very basic part of the modelling of the atmosphere's dynamics and chemistry. While two-flux, or, more generally, "two-parameter" approximations (Acquista et al[1]) to the radiative transfer equation are in common use for the energy budget computations, it is generally agreed that more advanced techniques are needed for the modelling of the chemical processes (Ruggaber et al[2]). In the present paper we discuss some current approaches to the solution of the radiative transfer equation in plane-parallel geometry and introduce the set of finite-difference algorithms which, while being as accurate as standard approximations, are naturally more efficient due to elimination of the eigenproblem solution step from their formulation.

The approaches considered here are in no sense new: their different implementations had been reported earlier (see, for example, Marchuk and Lebedev [3] and references therein), although they seemingly had not penetrated the meteorological community. In the following we shall try to show that these finite-difference approximations are more suitable for massive computations, that is, in the studies of the atmospheric energetics and chemistry as well as in retrieval applications than other solvers currently in use (Stamnes and Swanson[4], Nakajima and Tanaka[5], Rozanov et al[6], Moncet and Clough[7]).

Section 2 of the present paper is rather formal and is devoted to the numerical aspects of the problem. Here certain finite-difference approximations to the equation of radiative transfer in plane-parallel geometry are described. Their construction is based on "integro-interpolation method" (Samarskii[8] , Marchuk[9]) with certain modifications due to Fedorenko[10], the latter enforcing monotonicity of the computed solutions in case of optically thick layers. Importantly, integro-interpolation approach ensures the conservation on the algebraic level, that is, for an arbitrary vertical distribution of optical properties, in contrast with the "finite-difference method" from Lenoble[11], implementation of which is given in Ref(6). The difficulties encountered by the latter scheme in the presence of clouds are addressed in Kurosu et al[12], but, in general, when the optical properties of media experience rapid changes in vertical coordinate these approximations (and the method itself) do not seem to be truly adequate. That is because the conservation in this method is not guaranteed and only under very restrictive assumption on the coefficients of the equation the convergence could be proved.

Various angular discretisations are considered further and their applicability to the computation of fluxes and intensity field is addressed. Results of calculations in several simple test cases are presented, and the procedure for interpolation of intensity field to arbitrary angle or optical thickness is given. This part ends with performance estimates and a brief discussion of sources of numerical errors and potential remedies.

Section 3 is devoted to the development of the package for computation of radiative quantities and photodissociation rates in the Earth's atmosphere. Here the sources of spectroscopic and photochemical data are described and, in some cases, intercompared, adopted parameterisations and approximations are listed.

In section 4 comparisons of calculated clear sky NO_2 and $O_3 \rightarrow {}^1D$ photodissociation rates with observations are given and the off-line computations of the photodissociation rates for the European region are presented.

Uncertainties and various sources of errors are analysed in section 5.

In section 6 the summary of the obtained results is given.

The implementation of the package is described in the Part 2 of this report. It presents the description of the developed codes and user's manuals for the routines dealing with general radiative transfer, for those which handle and calculate optical properties and photodissociation rates, and those which do data manipulations.

Although we tried to make each part of the report self-contained, the reader should be warned that neither the first nor second part presents a complete review of the "state-of-the-art" techniques and methods.

2. Numerical aspects

This section deals with numerical algorithms which were implemented for the solution of radiation transfer equation in plane-parallel geometry. These include finite-difference variants of spherical harmonics and discrete ordinates which are best suited for the calculation of fluxes, fully discrete approximations for intensity field calculations, procedure for interpolation of intensity to an arbitrary angle and optical depth and quadratures for photodissotiaton rate computations. Potential for the improvement of numerical schemes is also addressed.

2.1 Formulation of the problem

We seek an approximate solution to the equation describing the transfer of non-polarized monochromatic radiation through the atmosphere of finite optical thickness H. For the plane-parallel case (Chandrasekhar[13])

$$\mu\frac{dI}{d\tau}+I=\frac{\omega}{4\pi}\int_0^{2\pi}\int_{-1}^{+1}G(\tau,\mu',\varphi',\mu,\varphi)I(\tau,\mu',\varphi')d\mu'd\varphi'+F(\tau,\mu,\varphi) \qquad (1)$$

where $I=I(\tau,\mu,\varphi)$ is specific intensity at level τ, τ is the optical depth $0\le\tau\le H$, μ- cosine of the zenith angle, positive for downward directions, φ - azimuth angle, positive counterclockwise with $0\le\varphi\le 360^\circ$, $G(\tau,\mu',\varphi',\mu,\varphi)$ - normalized to unity phase function, ω is the albedo for single scattering. For a parallel beam of light incident on top of a non-emitting atmosphere the right-hand side is

$$F(\tau,\mu,\varphi)=\frac{\omega S}{4\pi}G(\tau,\mu_0,\varphi_0,\mu,\varphi)e^{-\tau/\mu_0}$$

Here μ_0 is the cosine of the solar zenith angle and S is the intensity of the incoming beam. For the thermal radiation $F(\tau,\mu,\varphi)=\frac{1-\omega}{4\pi}B(T)$ with Planck's function $B(T)$. It is assumed that all relevant quantities are wavelength dependent.

The distribution of incoming diffuse intensity is specified at the top, $I(0,\mu>0,\varphi)=I_0(\mu,\varphi)$, and at the surface (for $\mu<0$)

$$I(\mu,\varphi)=2a_g\left(\int_0^{2\pi}\int_0^{1}\mu'(R(\mu',\varphi',\mu,\varphi)I(H,\mu',\varphi')d\mu'd\varphi'+F_g(\mu,\varphi,\mu_0,\varphi_0)\right)+S_g(\mu,\varphi) \qquad (2)$$

with $R(\mu',\varphi',\mu,\varphi)$ - surface reflection function for diffuse irradiance coming to the surface ($\equiv 1$ for an isotropically reflecting surface), a_g - the flux albedo, $F_g(\mu,\phi,\mu_0,\phi_0) = F_H Q(\mu,\phi,\mu_0,\phi_0)$ is the product of the intensity of the downwelling collimated illumination at the lower boundary with appropriately normalised reflection function for the collimated beam $Q(\mu,\phi,\mu_0,\phi_0)$ and S_g is the emission. This representation of the surface properties differs from the one traditionally adopted in remote sensing studies, but we feel that explicit sepration of the diffuse and direct irradiance at the lower boundary has certain technical (and computational) advantages.

Introducing zero- and first- order moments of intensity

$$A(\tau) = \frac{1}{4\pi} \int_0^{2\pi} \int_{-1}^{+1} I(\tau,\mu,\varphi) d\mu d\varphi \quad , \quad J(\tau) = \frac{1}{4\pi} \int_0^{2\pi} \int_{-1}^{+1} \mu I(\tau,\mu,\varphi) d\mu d\varphi$$

(called the actinic and net flux respectively), the balance relation may be easily obtained, which reads:

$$\frac{dJ}{d\tau} + (1-\omega)A = 0 \tag{3}$$

All finite-difference approximations considered below are designed in such a manner that the balance relation (3) holds. In other words, we shall study conservative methods only.

2.2 Standard approaches

Although a variety of the two- and four-flux methods had been presented in the literature (for example, Zdunkowski et al[14], Ref.(1), Li and Ramaswamy[15], Kylling et al[16]), we shall restrict our further discussion only to the higher order approximations to (1). The most advanced of the latter are the discrete ordinates formulations given in Refs.(4-5). These algorithms differ from the one originally proposed in Ref.(13) in certain computational aspects, most important being the use of shifted gaussian quadrature (Sykes[17]) and the manner in which the eigenproblem is solved.

Some alternative approaches to the angular discretisation had also been proposed. In the Ref.(1), the tensor product of piecewise-constant basis functions in μ and φ had been employed to form a Galerkin-type approximation to the equation of radiative transfer as a generalisation of the two-stream approximation of Schuster[18] (they called their basis "patch functions''). Another approximation had been given by Fricke[19] in the form of the composite quadrature. In the work of Kisselev et al[20] linear finite elements were used for discretisation in zenith angle, while Fourier decomposition was applied to separate the azimuthal dependence. All these authors used a spherical harmonics expansion of the phase function and eigensolver to facilitate integration in optical thickness. Here we shall only note that for the flux calculations the shifted gaussian quadrature and spherical harmonics expansion of the phase function seem more preferable than local (e.g., finite-element) approximations. For the intensity field calculations the situation is somewhat more complicated. See the section 2.7 for an example.

Obviously, the solution of the eigenvalue problem is rather expensive computationally. Also, the resulting linear system is often ill-conditioned so that pivoting is essential, which, in turn, makes the vectorisation hardly possible.

2.3 Finite-difference approximations

An enormous amount of methods had been invented for the solution of ordinary differential equations (Gear[21], Hall[22], Hairer and Wanner[23]). However, most of them cannot be regarded as quite satisfactory as they do not fulfill certain qualitative requirements such as conservation and monotonicity. For example, the trapezoidal rule when applied to a Cauchy problem for the model equation $y'=-ay$ produces recurrence $y_{k+1}=(1-0.5ha)/(1+0.5ha)y_k$. Obviously, for large ha the computed solution becomes oscillating and non-decaying (as $ha\to\infty$, $y_{k+1}\to -y_k$). By contrast, the first-order implicit scheme yields $y_{k+1}=1/(1+0.5ha)y_k$, which seems to be a "more physical'' approximation to the exponent $exp(-ah)$ at large steps h.

Routinely, the accuracy and monotonicity are maintained during the integration by monitoring the estimate of the local error and appropriate refinement of the integration step (see Refs.(21-23)). This seems hardly possible with the massive computations that we have in mind. Several other remedies are also known. In the "hybridisation'' approach (Ref.(10), also studied by many other authors as "variable step variable order" methods) the switching between schemes of different order is done when required by solution behaviour. Monotone (in the linear case) schemes (Butcher[24], Ref.(23), Kalitkin and Kuzmina[25]) turned out to be either too computationally expensive or relatively inaccurate (the method which performs excellently on the rapidly changing, e.g. "stiff" parts of the trajectory, is very often quite inaccurate when the solution behaves smoothly). Therefore the "hybridisation'' approach had been adopted in the current study.

The idea of the method may be illustrated by considering the system of linear ordinary differential equations with piecewise-constant coefficients

$$Y'=\mathbf{A}(\tau)Y+F(\tau)$$

with Y -unknowns and F -right hand side- vectors of length M, $\mathbf{A}$ -$M*M$ matrix, F and $\mathbf{A}$ defined at the midpoints of the grid intervals $[\tau_{k-1},\tau_k]$ for all layers $k=1,N$. After integration over the subinterval $[\tau_{k-1},\tau_k]$ one obtains the following set of algebraic relations:

$$\Delta_k Y = h_{k-1/2}\mathbf{A}_{k-1/2}\overline{Y_{k-1/2}} + h_{k-1/2}F_{k-1/2} \quad h_{k-1/2}=\tau_k-\tau_{k-1}$$

with the operators $\Delta_k Y=Y_k-Y_{k-1}$ and $2\overline{Y}_{k-1/2}=(1-Z_{k-1/2})Y_{k-1}+(1+Z_{k-1/2})Y_k$ standing for the difference and "average" respectively. Parameter $Z\in[-1,1]$ introduced in the definition of the average represents the trade-off between the order of approximation and monotonicity ($Z=0$ gives the trapezoidal rule and for $Z=\pm 1$ we have first order methods). In the following sections we shall apply this approach to various angular discretisations.

2.3.1 Spherical harmonics

We seek an approximate solution (I^{2M-1} approximation) to the radiative transfer equation (1) in the form

$$I^{2M-1}(\tau,\Omega)=\sum_{m=0}^{2M-1}(2m+1)\sum_{k=-m}^{m}\psi_{mk}(\tau)Y_{mk}(\Omega)$$

with unknowns $\psi_{mk}(\tau)$ and $Y_{mk}(\Omega)$ - spherical harmonics for solid angle Ω. The system of the ordinary differential equations for the rotationally symmetric part of the intensity field is written:

$$\alpha \frac{dJ}{d\tau} + \mathbf{a}\Psi = f$$
$$\beta \frac{d\Psi}{d\tau} + \mathbf{b}J = F \qquad (4)$$

with the vectors

$$J=[\psi_{2m+1}],\ \Psi=[\psi_{2m}],\ f=[(4m+1)F_{2m}]\ ,\ F=[(4m+3)F_{2m+1}],$$

diagonal matrices

$$\mathbf{a}=diag[(4m+1)(1-\omega g_{2m})] \text{ and } \mathbf{b}=diag[(4m+3)(1-\omega g_{2m+1})]$$

and bi-diagonal matrices α and β, which are independent of the vertical coordinate τ. In the above $g_m = \frac{1}{2}\int_{-1}^{+1} G(\mu)P_m(\mu)d\mu$, $F_m = \frac{1}{2}\int_{-1}^{+1} F(\mu)P_m(\mu)d\mu$, P_m is the Legendre polynomial of the order m for m=0,1,..

Two formulations of the boundary conditions are in use (with I being the sum of diffuse and direct intencities): the first belongs to Vladimirov[26] and Marshak[27] and the second is often called "the flux condition" (Gryn[28]). They are written, respectively, as

$$\int_0^1 P_{2i+1}(\mu)I(0,\mu)d\mu = 0 \quad \text{and} \quad \int_0^1 \mu P_{2i}(\mu)I(0,\mu)d\mu = 0 \quad \text{for each } i=0,1,...$$

These are the definitions for the top boundary. At the surface the definition is similar with obvious change in integration limits.

Integration of (4) over $[\tau_{k-1},\tau_k]$ gives the algebraic system

$$\alpha\Delta_k J + \mathbf{a}_{k-1/2}\frac{h_{k-1/2}}{2}\overline{\Psi} = f_{k-1/2}$$
$$\beta\Delta_k \Psi + \mathbf{b}_{k-1/2}\frac{h_{k-1/2}}{2}\overline{J} = F_{k-1/2} \qquad (5)$$

for each layer k=1,N , with operators $\Delta_k Y$ and $\overline{Y}$ defined earlier.

Boundary conditions lead to the algebraic relations of the form (for example, at the bottom boundary)

$$\sum_{m=0}^{M} c_{j,m}\psi_m = 0,\ j=0,1,..,\ m=0,1,...$$
$$with\quad c_{j,m} = (2m+1)\int_{-1}^{0} P_{2j+1}(\mu)P_m(\mu)d\mu \ \ or\ \ c_{j,m} = (2m+1)\int_{-1}^{0} \mu P_{2j}(\mu)P_m(\mu)d\mu \qquad (6)$$

The fact that matrices **a** and **b** are diagonal and α and β are independent of τ allows for the reduction of the order of the algebraic system at low computational cost. Through some school algebra we exclude J's from (5) and boundary conditions (6) to obtain an algebraic system with the block-tridiagonal matrix having twice less unknowns and blocks of size M*M. With some assumptions on the coefficients of the system it can be shown that the Gaussian elimination applied to it is stable (Ref.(3)).

2.3.2 Discrete ordinates

The angular discretisation for the m^{th} Fourier component Ψ^m of the solution is written

$$\mu_i \frac{d\Psi_i^m}{d\tau} + \Psi_i^m = \omega \sum_{j=0}^{2M-1} G^m(\mu_i, \mu_j)\Psi_j^m(\tau) w_j + \omega G^m(\mu_i, \mu_0) F_0 e^{-\tau/\mu_0} \qquad (7)$$

with μ_i and w_j being the nodes and weights of a certain (shifted Gaussian or some other) quadrature and for $L \geq 2M\text{-}1$ and $i,j = 0,2M\text{-}1$, $G(\mu_i, \mu_j) = \sum_{l=0}^{L} (2l+1) g_l P_l(\mu_i) P_l(\mu_j)$. A hybrid finite-difference approximation to (7) is constructed in a symmetric manner. Splitting the intensity in "upward" ($\mu < 0$) and "downward" ($\mu > 0$) components, we define averages as

$$\overline{2Y^{down}}_{k-1/2} = (1 - Z_{k-1/2}) Y_{k-1}^{down} + (1 + Z_{k-1/2}) Y_k^{down}$$

$$\overline{2Y^{up}}_{k-1/2} = (1 + Z_{k-1/2}) Y_{k-1}^{up} + (1 - Z_{k-1/2}) Y_k^{up}$$

Approximations of the boundary conditions and of the right-hand side are standard.

2.3.3 Fully discrete approximation

The angular discretisation is written:

$$\mu_i \frac{d\Psi_{im}}{d\tau} + \Psi_{im} = \omega \sum_{l=0}^{N} \sum_{j=0}^{2M-1} G_{ijml}(\tau) \Psi_{jl}(\tau) w_{jl} + F_{i,m}(\tau) \qquad (8)$$

where the integral term in (1) had been replaced by a certain quadrature with $\{\mu_i, \varphi_m\}$ being it's nodes, w_{im} - associated weights and $G_{ijml}(\tau) = G(\tau, \mu_i, \mu_j, \varphi_m, \varphi_l)$ - the original phase function at quadrature nodes. Rather often formulae of this type are defined as a "product" of one-dimensional quadratures with weights $w_{im} = w_i w_m$ (Davies and Rabinovitz [29]). Introducing the uniform grid in azimuth and applying discrete Fourier transform, the equations for each azimuthal component much like that in standard discrete ordinates formulation are easily obtained. We shall reference this approach as "quadrature" form of the fully discrete method.

Another possibility is to define a local tensor-product basis in $\{\mu, \varphi\}$ and apply standard finite element procedure (further referenced as "finite-element" form of the fully discrete method) to obtain an angular discretisation. From the computational point of view the piecewise-constant basis with an arbitrary grid in zenith angle and uniform grid in azimuth is the most reasonable choice. Then, for m-th discrete azimuthal component $\Psi^m(\mu)$ we have

$$\mu_{i+1/2} \frac{d\Psi_{i+1/2}^m}{d\tau} + \Psi_{i+1/2}^m = \omega \sum_{j=0}^{2M-1} G_{i+1/2,j+1/2}^m \Psi_{j+1/2}^m(\tau) w_j + \omega G_{i+1/2}^m(\mu_0) F_0 e^{-\frac{\tau}{\mu_0}}$$

with $G_{i+1/2,j+1/2}^m$, $G_{j-1/2}^m(\mu_0)$ evaluated appropriately (analytically, as in Ref.(1) or numerically by a certain quadrature).

The procedure outlined above differs from those previously proposed. The most important is the use of original phase function instead of it's polynomial approximation (contrary to Refs.(1,19)). The stability constraints are much relaxed for the finite-element formulation compared to the

straightforward discretisation especially in case of strongly peaked phase functions. The vertical discretisation and solution procedures are the same as for discrete ordinates.

2.4 Accuracy estimates and performance

In this section some numerical evidence will be provided. As a tool for comparison, the DisORT solver was chosen (although DisORT version 1 had been communicated to the author by Dr. S.-C. Tsay, in all experiments we used DisORT version 2 (prerelease), communicated to author by Dr. J.Key with the STREAMER[30] package). With chemistry-related applications being the primary motivation of the present work, the main emphasis will be given to actinic flux computations in the short-wave spectral region, although some problems regarding the representation of the intensity fields will also be addressed. DisORT runs were done in double precision, all finite-difference approximations - in single precision. The computations were performed on a workstation with 4-byte reals.

2.4.1 Homogeneous slab

In order to make the comparisons of the methods outlined in previous sections more straightforward, we start with the simplest test problem. Namely, we calculate radiative quantities in a homogeneous slab of optical thickness H = 1 with non-emitting isotropically reflecting bottom boundary with flux albedo a_g= 0, for a beam source of intensity 1 at top. Values of other defining parameters varied: cosine of the beam incidence angle μ_0 = (0.25, 0.55, 0.85), single scattering albedo ω = (0.8, 0.9, 1.0), asymmetry factor g=(0.7, 0.8, 0.9). The computations were performed with Raleigh $R(\cos\gamma) = 1 + 0.1\cos^2\gamma$ and Henyey-Greenstein $H(g,\cos\gamma) = \frac{1-g^2}{(1-2g\cos\gamma+g^2)^{3/2}}$ phase functions with N=20 layers in optical thickness and M = (2, 4, 6, 12, 24) discrete fluxes. In runs with M=24 two additional levels were added near the boundaries. Computations with $M < 24$ were performed with the δ-M modification of Wiscombe[31]. As "exact" values, the results obtained from DisORT run with 48 discrete fluxes were taken. The error for M^{th} order approximation was defined as $E_M = \max_{\mu_0,\omega,g} \int_0^1 \frac{|A(\tau) - A_{exact}(\tau)|}{A_{exact}(\tau)} * 100\%$ with the maximum taken over all values of μ_0, ω and g.

In Table 1 the errors E_M in approximation of actinic flux for DisORT, finite-difference discrete ordinates, spherical harmonics (for both types of boundary conditions), N-stream generalisation of Schuster's method (differing from the form proposed in Ref.(1) in the manner in which integrals with "patch" functions were evaluated) and two variants of the fully discrete method are shown for different angular resolutions.

Table 1 Percent errors in acinic flux for the homogeneous slab test

METHOD	ANGULAR RESOLUTION				
	2	4	6	12	24
DisORT ♣	15.4	6.9	1.8	0.5	0.02
Discrete ordinates	15.9	6.9	1.8	0.4	0.1
Spherical harmonics (Vladimirov-Marshak)	17.7	12.2	7.8	1.0	0.3
Spherical harmonics ("flux" boundary)	17.7	10.7	6.3	3.5	3.0
N - Schuster (Ref.(1))	15.4	11.8	7.4	1.9	0.4
Fully discrete -"finite elements"	17.5	11.2	4.0	1.4	0.4
Fully discrete -"quadrature "	90.0	69.2	38.2	8.1	1.2

In general, results from the finite-difference variant of discrete ordinates and DisORT were practically indistinguishable. Spherical harmonics were less accurate than discrete ordinates because of the influence of discontinuity imposed by boundary conditions. "Flux" boundary conditions performed better for coarse resolutions, but Gaussian elimination (without pivoting) applied to the relevant linear systems turned out to be subject to more roundoff (on a computer with short mantissa). To avoid severe stability constraints inherent to the "quadrature" form of fully discrete method, the device recommended by Kantorovich and Krylov[32] for the solution of integral equations with singular kernel had been used. For coarse resolutions the fully-discrete "quadrature" method is clearly inedequate. It should be noted, however, that for the smooth phase functions or at very high resolutions the "quadrature" method may be as accurate as discrete ordinates. Total set of computations had been repeated with ground albedo a_g =0.9. The performance of the spherical harmonics (with both types of boundary conditions) improved. Nevertheless, they had not reached the accuracy obtained by dicrete ordinates. For all methods tested the largest errors were located in the grid cells next to the boundaries. Mean (over all cases) errors were about 1.5-2 times smaller. This test made it possible to select methods for further experimentation. These are: finite-difference discrete ordinates (the most accurate), spherical harmonics (which are about twice faster than all other finite-difference methods) and both forms of the fully discrete method ("finite-element" form being the more robust and "quadrature" form to provide links with the standard discrete ordinates approximations). While the first two seem to be most suitable for flux calculations, the fully-discrete methods were used in the calculations of the intensity field.

2.4.2 Ozone column

Data for this test had been communicated to the author by J.Landgraf (for motivation of the problem see Landgraf[33]).). Actinic flux had been computed for 7 distributions of optical thickness and single scattering albedo given on 62 levels in the clear atmosphere (Raleigh phase function), with ground albedo a_g =0 for μ_0=(0.5001,1.0). These distributions were generated for some specific profile of absorbers and the wavelengths ν =(205.13, 287.77, 302.00, 320.00, 370.00, 580.00) nm. Angular resolutions M=(2,4,6,12) were used. As "'exact" results from M=24 DisORT calculation were taken. In the following Table 2 the error $E_M = \max_{\mu_0,\nu} \int_0^1 \frac{|A(\tau) - A_{exact}(\tau)|}{A_{exact}(\tau)} * 100\%$ is given for different angular resolutions.

♣ Version 2 !!!

Table 2. Percent errors in actinic flux for the ozone column test

METHOD	ANGULAR RESOLUTION 2	4	6	12
DisORT	14.8	3.8	1.9	0.3
Discrete ordinates	14.4	3.8	1.9	1.3
Spherical harmonics	16.3	7.3	4.1	2.3

Again, spherical harmonics (with Vladimirov-Marshak boundary conditions) were least accurate. In coarse resolution the accuracy is slightly better than in the previous test. Slowing of convergence of the discrete ordinates for higher resolutions is explained by the violation of constraint inherent to all finite-difference approximations of the equation (1): the step in optical thickness should decrease with increasing angular resolution (see Ref.(3)). Only then the asymptotic convergence is guaranteed. The proportionality constant in this constraint depend on the order of accuracy of the difference scheme in the vertical coordinate and itself decreeases with the increasing order. In this `particular case the addition of one or two extra layers cures the problem.

2.4.3 Standard atmospheres

In this experiment we tried to estimate an error in actinic flux computations for 6 standard atmospheres: tropical, midlatitude summer and winter, subarctic summer and winter and US-standard (Anderson et al[34]). Computations were performed for 8 diffuse spectral albedoes referring to the 8 surface types: summer and spring grass, forest, water, sand, old and fresh snow, savannah, which were compiled from various sources (references include STAR dataset,- A. Ruggaber, personal communication, STREAMER dataset,- Ref.(30) etc). Optical parameters were μ_0= (0.25, 0.55, 0.85), column optical thickness of background aerosol (at wavelength ν_0=550 *nm*) τ_{550} = (0.0, 0.5, 1.0). Wavelength grid with 78 points distributed within [290-690] *nm* interval was used. Gaseous absorbers were O_3, NO_2, SO_2. Vertical aerosol profiles had been fixed. Phase functions for aerosols (average continental in lower troposphere, clean continental in troposphere and stratospheric, d'Almeida et al[35]) were produced via Mie calculations. The aerosol parameters for this experiment has been communicated to the author by A. Ruggaber as part of the STAR package (A. Ruggaber, personal communication). Calculations were performed with M=(2,4,6,12) discrete fluxes/moments on N=32 levels in the vertical. As "exact" we took results from the M=24 finite-difference discrete ordinates calculations. In the following Table 3 the error $E_M = \int_0^1 \frac{|A(\tau) - A_{exact}(\tau)|}{A_{exact}(\tau)} * 100\%$ in the frequency integrated actinic flux is given for 3 aerosol cases with the maximum taken over all surface types, solar zenith angles and atmospheric profiles which were used in the computations.

Table 3. Percent error in actinic flux for the standard atmosperes test

METHOD, CASE	ANGULAR RESOLUTION 2	4	6	12
Discrete ordinates, τ_{550} = 0.0	11.2	3.4	1.1	0.1
τ_{550} = 0.5	12.0	2.5	1.0	0.1
τ_{550} = 1.0	10.3	2.2	1.2	0.2
Spherical harmonics, τ_{550} = 0.0	12.9	6.2	4.1	1.8
τ_{550} = 0.5	15.9	6.1	3.4	1.3
τ_{550} = 1.0	14.0	5.6	3.2	1.2

This test had shown that the error in the frequency integrated actinic flux is rather reasonable even for the coarse angular resolutions and large amounts of aerosols. Errors in the heating rate are of the same order. For chemistry-related applications, however, this is not enough. Since we have to calculate integrals over portions of the spectra, the spectral behaviour of the error becomes important. Other numerical experiments have shown that the relative accuracy of actinic flux approximation in the [290-340] *nm* region is rather poor as it is very sensitive to variations in optical properties of aerosols caused by the variations in relative humidity profiles. Also, the purely numerical problems related to step size constraints come into play. On the other hand, the importance of these errors may be argued because the absolute values of photodissociation rates are rather small for these spectral regions.

2.5 Calculation of the photodissociation rates

The photodissociation rates for the j-th atmospheric constituent are defined (Madronich[36]) as integral over all wavelengths of a product of actinic flux, absorption crossection and certain rather well behaved quantity which is called the quantum yield. We shall use the form proposed in Ref.(2)

$$R_j(z) = \int_{\nu_1}^{\nu_2} S(\nu)\sigma_j(T,P,\nu)Y_j(T,P,\nu)A(z,\nu)d\nu \tag{9}$$

where ν is the wavelength, T- temperature, P- pressure, $\sigma_j(T,P,\nu)$- absorption crossection, $Y_j(T,P,\nu)$- quantum yield, $S(\nu)$- solar flux at the top of the atmosphere. For the evaluation of integrals (9) an efficient quadrature rule of product-integration type (see Ref.(29)) had been designed. The idea is the following. Consider an interpolatory approximation to the actinic flux on the whole interval $[\nu_1,\nu_2]$: $A(z,\nu) = \sum_{k=1}^{K} A(z,\nu_k)\phi_k(\nu)$ with $\phi_k(\nu), k = 1,K$ being an appropriate set of functions forming basis in $[\nu_1,\nu_2]$, say, B-splines (de Boor[37]). Inserting the expansion into (9) and integrating product $S(\nu)\sigma_j(T,P,\nu)Y_j(T,P,\nu)$ with the k-th basis function we obtain a very simple and efficient integration rule. With the B-splines fixed as a basis for interpolation only the wavelength grid remains to be defined. It is not very difficult, when one has a couple of high-resolution calculations. Unfortunately, this approximation is definitely not optimal, so further improvements are possible. See Gautschi[38] for the algorithms for construction of Gauss-type quadrature rules.

2.6 Wavelength grid

To estimate the number and distribution of points required for wavelength integration, computations (standard atmospheres test) were performed using nonuniform wavelength grids with 16, 23 (grid spacing from Ref.(2)), 78, 96 and 124 points, the results from the latter case taken as "exact". As a measure of inaccuracy we took maximum of a relative error over all optical parameters (as in section 2.4.3) and 21 reaction rate that were computed (for the list, see Part II). Resolutions of 78 and more nodes were practically indistinguishable from the "exact" case, 23 and 16 nodes gave an error below or about 10%. Currently we are using the 78 nodes resolution. A grid with 16 properly distributed nodes seems to be good choice in terms of accuracy and efficiency, but as the problem is inherently statistical, the final decision is postponed to the moment when enough experimental data will be gathered.

2.7 Calculations of intensity

Generally, all methods that were listed in section 2.3 are suitable for the intensity field calculations. In this section only two of them will be compared, that is, DisORT and the fully discrete approximation in the quadrature form. As has been mentioned earlier, the latter may be used for relatively smooth phase functions. The intensity field was computed within homogeneous slab of optical thickness 1 with the Heney-Greenstein phase function (g=0.7), low-reflecting surface (a_g =0.1), $\omega = 0.9$ and beam source of intencity 1 incident at the top boundary at $\mu_0 = 0.5, \varphi_0 = 45^\circ$. In both methods M=64 discrete fluxes and 64 levels in the vertical coordinate were used. To facilitate the comparison of methods, intensity distributions were produced at the Gaussian quadrature points in μ and on the uniform grid in φ. Reflected and transmitted intencities at top and bottom of the slab, respectively, are plotted in Fig.(1) as a function of the cosine of the zenith angle ($-1 < \mu < 0$ for transmitted at bottom boundary and $0 < \mu < 1$ for reflected at top boundary) for φ=45°.Fully discrete approximation is labelled "FD". The agreement between the methods is good. Next Fig.(2) gives intensity distribution for another azimuthal angle, φ=225°. DisORT values are almost twice smaller for this case. Calculations performed with higher angular/vertical resolutions produced practically the same results. The only possible explanation is that the use of the Legendre expansion of the phase function even in this very simple case leads to an erroneous determination of the transmitted/reflected intensity fields in the azimuthal directions other than that of the incident beam. Further numerical experiments have shown, that these deviations increase when the phase function becomes more stretched. Finally, experiments with degenerate phase functions (that is, the number of nonzero terms in their's polynomial expansion is constant while the number of discrete fluxes increase) have shown perfect agreement in the intensity distributions obtained from both methods.

2.8 Angular interpolation

Following Vladimirov[39] and Ref.(3), we rewrite the equation (1) along the arbitrary direction $\xi=\tau/\mu$. Then

$$\frac{dI}{d\xi} + I = Q(\mu\xi, \mu, \varphi) \tag{10}$$

with the source function

$$Q(\mu\xi, \mu, \varphi) = Q(\tau, \mu, \varphi) = \frac{\omega}{4\pi} \int_0^{2\pi} \int_{-1}^{+1} G(\tau, \mu', \varphi', \mu, \varphi) I(\tau, \mu', \varphi') d\mu' d\varphi' + F(\tau, \mu, \varphi) \tag{11}$$

Considering $Q(\tau, \mu, \varphi)$ to be a known function one easily obtains the formal solution of (10), which is

$$I(\xi) = I(\tau, \mu, \varphi) = I_0 \exp(-(\xi - \xi_0)) + \int_{\xi_0}^{\xi} Q \exp(t - \xi) dt \tag{12}$$

Suppose now that on the interval $[\xi_0,\xi_1]$ of length $h=\xi_1-\xi_0$ the function $Q(\xi)$ could be sufficiently well approximated by the linear expression $Q(\xi)=h^{-1}((\xi-\xi_0)Q_1+(\xi_1-\xi)Q_0)$. Then, evaluating (11) at ξ_1, one easly obtains $I_1=pI_0+qQ_0+(1-p-q)Q_1$,where p=exp(-h), q=(1-exp(-h))/h-exp(-h). This relation is monotone. Now the intensity at arbitrary angle and optical depth could be found by a marching procedure starting from the appropriate boundary, provided one has a good estimate of Q

at required μ,φ. This amounts to evaluating the source function at a set of new angles and summation.

The primary assumption (and the main source of errors) in the outlined scheme is the linearity of the function (11). Although more accurate procedures may be designed (see Ref.(3)), the listed formulas are consistent with the piecewise-linear approximations used in the present work.

2.9 Performance

Finite-difference methods are generally more efficient than those labelled above as standard. Among them the spherical harmonics are fastest. Performance of both variants of fully discrete method and "*N*-Schuster" method was about the same as finite-difference discrete ordinates. These estimates were obtained primarily on scalar hardware and they reflect the difference in the number of operations among the advocated and standard approaches, as no hardware- or compiler-specific tuning had been done. Actually, timings were obtained in the course of numerical experiments described in previous sections. For angular resolutions higher than 4, spherical harmonics were approximately 90 times faster than DisORT, but substantially less accurate. On the other hand, finite-difference discrete ordinates, while maintainig the same level of accuracy as DisORT, were about 30 times faster than the latter. Another scalar comparison has been made with the 6-flux variant of the matrix operator code (Ref.(5)) supplied with STAR package (Ref.(2)). This program was approximately 4 times slower than DisORT.

Some limited comparisons were done on Cray-YMP (1 processor) using PerfTrace utility. LINPACK routines from Cray Scientific library had been used with DisORT. Again, no attempt was made to tune finite-difference methods to specific hardware or optimise them for specific resolution. Actually, we used the same code as for scalar runs. With 4 discrete fluxes, finite-difference discrete ordinates were 230 times faster than DisORT, with 6 fluxes - 140 times faster. Spherical harmonics were, respectively 600 and 470 times faster. The radiation kernel of the STAR package was 1170 times slower than discrete ordinates and 3900 times slower than spherical harmonics. The vector performance of the proposed algorithms matches that reported for the CHARTS code (Ref.(7)).

3. Physical parameters

The development of a general purpose package for radiative transfer is impossible without careful reassessment of the available data, parameterisations and models for the physical processes involved. In this section we state main decisions made in this work, and, in some cases, estimate their impact on the accuracy of the computed values. Only the shortwave ([200-700] *nm* region) properties are considered below.

3.1 Extraterrestrial Solar Spectrum

In this work the extraterrestrial solar spectrum as given by Kurucz[40] and supplied with MODTRAN[41,42] package has been implemented. We use the version with 5 cm^{-1} spectral resolution specified for the range [50000 -200] cm^{-1}. An option exists for the use of 1 cm^{-1} resolution version.

3.2 Rayleigh scattering

For Rayleigh scattering the set of formulae proposed by Edlen[43] was implemented. With ν-wavelength in μm, the refractive index of CO_2-free air at 1013 hPa and 15°C is given by the following relation (Ref.(43))

$$10^{-8}(n-1)_{CO_2-free} = 6431.8 + \frac{2949330}{146-\nu^{-2}} + \frac{25536}{41-\nu^{-2}}$$

Carbon dioxide correction (ζ - the volume mixing ratio of CO_2) is (Ref.(43))

$$(n-1)_{standard\ air} = (1+\varsigma\frac{n_{CO_2}-n_{air}}{(n-1)_{air}})\cdot(n-1)_{CO_2-free}$$

which gives a factor which is approximately constant to the required accuracy (Koch[44]) and for 0.03% of CO_2 equals 1.000162.

Pressure, temperature and humidity dependence are incorporated by

$$(n-1)_{TPE} / 1.33289 = (n-1)_{standard\ air}\frac{0.00138823\cdot P}{1+0.003671\cdot(T-273.15)} - E\cdot(5.722-0.0457\nu^{-2})\cdot 10^{-8} \qquad (13)$$

Here P is pressure (hPa), T- temperature (°K), E is the water vapor pressure (hPa) and the formula is taken from Frolich and Shaw[45]. Finally, the Rayleigh extinction coefficient for anisotropic molecules is given by the following formula (Kerker[46])

$$k_R = 24\frac{\pi^3}{\nu^4}\cdot\frac{6+3\cdot\delta}{6-7\cdot\delta}\cdot\left(\frac{n^2-1}{n^2+1}\right)^2 N^{-1}$$

Here k_R is the Rayleigh scattering coefficient (m^{-1}), ν is the wavelength (m), N is the number density of air (m^{-3}), n is the pressure and temperature dependent (what is "...understood but often forgotten" - Penndorf[47]) refractive index of air and δ is the (dimensionless) depolarisation factor. The estimates for the latter quantity vary from 0.0095 (Ref.(45)) to 0.035 (Hoyt[48]) with the value 0.0279 recommended by Young[49] (see also Bakan and Hinzpeter[50]), the one that was used in the computations. The wavelength dependence of the depolarisation factor was also reported by Bates[51], with it's value growing toward shorter wavelengths. At the same time, various other formulae for $n_{standard\ air}$ (Peck and Reeder[52], see Teillet[53] for comparison) produce values that are practically indistinguishable in the wavelength region of interest. We were using the formula from (Ref.(45)) with pressure and temperature dependence given by (13). Humidity dependence is negligible in the UV-visible wavelength range and was not accounted for. We note that pressure, temperature and humidity dependent refractive index of air is implemented in Ref.(42) based on Edlen[54] definitions.

The temperature and pressure correction (13) is rather important. Although, as numerical experiments suggest, it's influence may be masked by aerosol scattering. Nevertheless, this correction redistributes heating rates in the atmosphere, as can be inferred from Fig.(3), where the percent difference in the averaged over 6 standard atmospheres, 8 surface types and 3 values of the zenith angle heating rate is presented for the pressure-dependent and independent refractive index of air (all parameters were from the test case "standard atmospheres" from section 2.4.3, "clear case"). What seems to be more important for the present study, NO_2 photodissociation (beleived to be the main ozone generator) is about twice larger in the troposphere and smaller in stratosphere. See Fig.(4) for average deviations of calculated NO_2 and $O_3 \rightarrow (^1D)$ dissociation rates in the clear

air case. Addition of aerosols decreases the absolute magnitude of these deviations almost uniformly with height, and for τ_{550}=0.5 they are approximately two times smaller. We shall return to this topic in the following sections, where further numerical evidence will be provided.

3.3 Absorption crossections

The problem of an accurate determination of the absorption crossections of various gases in the UV-visible region of the spectrum has received significant attention in the recent years. Malicet et al[55] measured the ozone absorption crossection in the spectral range [195-345] *nm* for the temperatures 218, 228, 243, 273 and 295 °K and compared them with results obtained by Yoshino et al[56,57], Molina and Molina[58], Bass and Paur[59] and Cacciani et al[60]. Measurements of Ref.(58) are reported to be on average 1.5-3.5 % greater for wavelengths larger 240 *nm* , Ref.(59) was in exellent agreement for wavelengths not exceeding 310 *nm* , but for larger wavelengths shifts of +0.05*nm* were observed (Ref .(55)). Currently, values from Ref.(58) are used in the Hartley and Huggins bands, with an option of replacing them with data from Ref.(59).

Another important absorber in the spectral range of interest is nitrogen dioxide. Rather extensive compilation of existing measurements is given in Kirmse et al[61] for the spectral range 300-700*nm* with resolution 0.05 *nm* and for larger wavelenghts with resolution of 1 *nm*. In the range 300-500 *nm* absorption crossections were measured at ambient and low temperatures by Merienne et al[62], Coquart et al[63], Jenouvrier et al[64]. Approximately at the same time different measurement techniques were used by Vandaele et al[65] and Harder et al[66] The latter work also demonstrated pressure dependence of high-resolution spectra of NO_2. All these results are in very good agreement with each other. On the other hand, DeMore et al[67] recommend temperature dependent values from Davidson et al[68] , which are given at approximately 5 *nm* resolution for the range 202-422 *nm*. In the numerical experiments reported further we used values from Schneider et al[69] which were at the bottom of the list in the comparisons cited above, primariliy due to the spectral shifts in the measurements. In the current version of the package the O_3 and NO_2 absorption crossections as given in Burrows et al[70] and Burrows et al[71]. are implemented.

Sulfur dioxide and oxygen are less important for the tropospheric chemistry. Nevertheless, we incorporated their absorption crossections based on data described in Refs.(67,2,36). For all other species (NO_3, N_2O, HNO_2 ,HNO_3, HNO_4, H_2O_2, CH_2O etc) the data from EURAD-CTM (Chang et al[72], Stockwell et al[73]) is used.

3.4 Aerosols

Aerosols are very important components of the Earth's atmosphere with respect to radiation processes. At the same time, as noted in the MODTRAN report (Ref.(41)), the seemingly simple question "Which [aerosol] model should be used for what location and weather situation ?" is difficult to answer precisely. While within the boundary layer (lower 2 km) aerosols are controlled by the local sources, geography and weather conditions, in the upper troposphere (2 to 10 km) the seasonal variations are beleived to be the dominating factor (Hoffman et al[74].). Background stratospheric (10-30 km) aerosols are considered to be mostly composed of sulfate particles formed by photochemical reactions. However, the loadings of stratospheric aerosols are occasionally increased by a factor of about 100 following massive volcanic eruptions. There is also seasonal and geographical variation in stratospheric aerosol profiles related to the height of the tropopause (Ref.(74)) The aerosol properties and vertical distributions in the upper atmosphere are very uncertain. In the current version of the package the aerosol models provided with the STAR (Ref.(2)) package are being used. They include rural, clean continental, urban, desert, maritime and

background tropospheric and stratospheric aerosols. Optical parameters for all these were derived via Mie calculations based on the d'Almeida et al[75] and Ref.(35) refraction index data. Spectral and humidity dependence of the optical parameters is accounted for. Several first moments of phase functions are used in radiative transfer calculations. It should be noted that the use of the asymmetry factor as a single parameter describing phase functions (as in Koepke et al[76]) may not be adequate for computations related to photochemistry due to the strong backscatter exhibited by at least some of the aerosols (Mishchenko et al[77], Ref.(75)). In the current version the wind-dependent desert and maritime aerosol models are implemented based on Ref.(41)) data. Implications of the sulfate aerosol resulting from Mt. Pinatubo eruption on the stratospheric photochemistry were studied in a number of articles (Kondo et al[78], Rosenfield et al[79], Huang and Massie[80]). The volcanic aerosols influence tropospheric photochemistry in two ways: first, modifying the downwelling radiation through the additional scattering in the cloud located in the lower stratosphere, and second, through radiative interaction with the tropospheric clouds. Numerical experiments (not shown) indicate that the second mechanism is, generally, much stronger. For the optical parameters of the stratospheric sulfate aerosols the data given in Ref.(80) and Stenchikov et al[81] was used.

3.5 Clouds

Representation of cloud optical properties is based on several sources. A set of parameters from the STAR package (Ref.(2)) is used as well as parameterisations from ECHAM-4[82] and the meteorological model of the German Weather Service (further referenced as DWD, see Jacob and Podzun[83] for description). The STAR data represent a sort of a lookup table where for different cloud and fog types (several Cumulus types, Altostratus, Nimbostratus, Stratus, Maritime Stratus, Straticumulus, Ice Cloud, Radiation Fog) the wavelength dependent extinction and phase functions are given. This set can be used for the cases when type of cloud and the number of droplets are known or prescribed. Meteorological and climate models, on the other hand, produce as primary cloud-related variables the liquid water content and, as a rule, diagnostically, cloudiness fraction and effective droplet/ice crystal radius. Therefore the parameterisations from ECHAM-4 for ice and water clouds were incorporated for derivation of extinction coefficient and asymmetry factor based on the works of Johnson[84] and McFarlane et al[85]. These parameterisations are in good agreement with those from Hu and Stamnes[86]. The DWD parameterisations, which are based on semi-empirical formulae, are used for the diagnostic determination of the vertical distribution of liquid water content and cloudiness fraction when the output of DWD model is used as meteorological driver for chemistry-related applications (the option for using DWD fields with CTM was introduced by B. Langmann). When STAR cloud parameters are used, the droplet/crystal number concentration should be specified. Otherwise, unrealisitcally high optical thicknesses of clouds mayl result (as in Hass and Ruggaber[87]).

When partial cloudines is diagnosed in the grid cell, we use weighting of the source term to produce "effective" single scattering albedo, extinction coefficient and phase function moments for the whole cell. This approach has something in common with those proposed in Gabriel and Evans[88], but, of course, is very crude. For high sun it seems to produce qualitatively correct results while the cell sizes remain relatively large. Side illumination effects and nonlocal approximations were not considered in the present work. Nevertheless, with the introduction of the new generation of numerical weather prediction models, they are becoming more and more important (Ritter[89]).

3.6 Interaction of clouds and aerosols

It is well known that aerosols can significantly perturb cloud optical properties (see, for example Ackerman and Baker[90] for rather early discussion of the problem). Hygroscopic growth and phase partitioning of particles and the resulting change in optical properties in highly humid environments has been studied experimentally (Svenningsson[91], Hallberg[92]) and theoretically[93]. These studies (as well as other related experiments, see, for example, Svenningsson et al[94]) indicate that two groups with different hygroscopic properties could be detected in the internally mixed aerosols. Also, nucleation scavenging of aerosol particles as a function of particle size could be described by hygroscopic growth spectra (Ref.(94)). For the modelling of these processes the chemical composition of the aerosols as well as the size distribution are to be known. The *S*-shaped partitioning curve wich was detected in these and other (Noone[95]) experiments seems to be relatively insensitive to the time particles stay in cloud, but is shifted with respect to the different airmass origin and aerosol composition. Since the latter parameters are highly uncertain in the framework of the current meteorological models, we do not account for these effects, as well as for changes in optical properties of the water droplets due to the scavenging/solution of solid particles. To be incorporated in the radiation codes suitable for massive computations, these effects require additional consideration. Currently, only case-based numerical experiments made together with elaborate microphysical models are possible.

To summarise, optical properties of polluted cloud are determined by (a weighted sum of): pure water drops/ice crystals, drops/cristals with solid inclusions or solutions, their number determined by physico-chemical properties of particulate matter and size distribution, and the aerosol particles modified by high humidity. The complexity of the models involved inhibit the inclusion of such processes (at least at this stage of experimental and teoretical development) in the general-purpose radiation code. The study of the radiative properties of ice crystals containing scattering as well as highly absorbing inclusions performed by Macke et al[96] indicate that "independent scattering approximation, where the separately calculated scattering properties of ice and inclusions are simply added do not give satisfactory results" (see ref). In other words, wintertime radiative transfer calculations in industrial regions should define polluted ice/water clouds as special types of absorbers.

3.7 Surface properties

Several sources of data were used to obtain spectrally dependent albedi for various surfaces. Again, the STAR (Ref(2)) and STREAMER (Ref.(30)) (see Bowker et al[97], Eaton and Dirmhirn[98], Tanre[99] for the data references) packages turned out to be very useful and (as surface types implemented in them overlap) provided certain basis for verification. The model for reflection (glitter) from water surfaces was taken from McLinden et al[100], although the wavelength dependence given in this article seems to be somewhat less consistent with data from other sources. Attempts to estimate anisotropy in clear-sky albedoes for desert scenes were reported by Capderou[101]. Still, more experimental evidence is required. The partial snow cover and broken ice/water surfaces were not implemented.

3.8 Photochemical parameters

The quantities of primary importance to the photochemical computations are the quantum yields. While the quantum yield for NO_2 dissociation seems to be rather well established (Gardner et al[102],Ref(67)), the photodissociation rates of ozone had been reassessed recently (Michelsen et al[103], Muller et al[104], Ball and Hancock[105]). Recommended values from Ref.(67)are in qualitative

agreement with those given by Michelsen et al (Ref.(103)), if one interprets "kT" in the denominator of formula (5) from Ref.(103) as T°K. In the present work, the recommended values (Ref.(67)) vere used. In Fig.(5) the calculated photodissociation rates for $O_3 \rightarrow {}^1D$ channel are compared for the recommended values (Ref.(67)) of the quantum yield and those given in Ref(36) for the midlatitude summer atmospheric profile and two aerosol loadings, (clear and with aerosol optical thickness at 550 *nm* of 0.5). The pressure dependent refraction index of air was used in these computations. The distance between curves in Fig.(5) may serve as an indicator of the influence of uncertainty in the $O_3 \rightarrow {}^1D$ quantum yield on the relevant reaction rate.

For all other reactions considered (the set of reactions coincide with that adopted in Refs.(72,73)) the values and parameterisations from EURAD-CTM (Refs.(72,73)) and Ref.(2) were used.

3.9 Meteorological drivers

The current version of the package provides interfaces to the meteorological data produced by HIRLAM[106] and DWD models.

4. Comparisons with site observations and CTM model

Measurements of the photodissociation rates have been made by various authors in a multitude of locations and atmospheric conditions. To mention only few, O_3 and NO_2 dissociation rates were studied in the works of Dickerson et al[107], Parrish et al[108], Jaegle et al[109], Feister[110] , McElroy et al[111], Kelley et al[112], Dickerson et al[113]. Various formulae were proposed to aproximate NO_2 reaction rates at surface (Refs.(107,108,110)) or it's change with height (Ref.(112)) in clear-sky conditions. Several of these measurements were selected for comparison. Accurate comparison of measured and calculated photodissociation rates is greatly complicated by the fact that these quantities are very sensitive to the scattering properties of the atmosphere, that is, to the loading and height distribution of the aerosols which are normally obtained through some retrieval procedure (Ref.(113)). As pointed out in the work of Mishchenko (Ref.(77), even moderate nonsphericity of the aerosol particles can cause large errors in the retrieved optical properties of aerosols, when the standard Mie theory is used in the algorithm. More importantly, there is no cancellation of errors when these retrieved properties are inserted in radiative transfer calculations. Therefore, computational results will be presented for a range of aerosol loadings and ozone vertical distributions. At the same time, we keep the vertical distribution of aerosol fixed throughout all the computations and corresponding to that used in the "standard atmospheres" test.

4.1 Measurements of Kelley et al[112]

The difficulties addressed in the above discussion are highlighted in comparison with observations of Ref.(112), where airborne measurements were made for clear-sky conditions, low surface albedo and a range of heights from 0.2 to 7.5 km in research flights over rural southwestern US. Reported average aerosol loading was "27 $\mu g/m^3$ below 1.5 km and orders of magnitude less above that altitude". The ground albedo was estimated to be 0.085. The polynomial fit for the measured $j(NO_2)$ for the solar zenith angle of 58° was provided. The total uncertainty at 95% confidence level was estimated to be 6%. In Fig.(6) the difference in measured and calculated $j(NO_2)$ for *clear* (zero aerosol loading) atmospheres with different vertical ozone distrbutions is presented. The pressure and temperature *independent* refraction index of air was used in these computations. On average, the agreement is well below the experimental error. Addition of aerosols introduces a systematic shift in the calculated $j(NO_2)$, thus increasing the average discrepancy. Although with

certain modifications in the optics of the added aerosols we might combat that, we preferred to keep their properties fixed. In Fig.(7) results of computation with the pressure and temperature *dependent* refractive index are compared with observations, again, for several atmospheric profiles of ozone, and two aerosol loadings, with the column optical thickness at ν=550 *nm* being 0.06 and 0.09 (at ν=330 *nm* approximately 1.5 times larger). Since there are more sign changes in the error the agreement should be considered to be better than in the previous case. The curves in these two figures are labelled according to the following scheme: each case is indexed by a triplet of integers IJK, where I-is the ordinal number of the aerosol case (0-no aerosol,etc), J- refers to the ordinal of the atmospheric profile used (tropical etc), K - is the surface type number (in this test surface albedo was 0.085 for all wavelengths, so only aerosol loading and ozone profiles varied). Qualitatively, the addition of scattering material shifts the pressure-dependent curve towards higher values. At this point we stop "tuning", as it is obvious now that, by modifying the aerosol vertical distribution, agreement to any desired accuracy could be reached. These figures may also be used for qualitative assessment of the combined effect of ozone profile and aerosol loading changes. Another implication is that the pressure-independent refractive index of air, however it may sound rather absurd, could be used to mimick ("simulate") the low aerosol backgrounds in the troposphere. We shall return to these questions in the following sections.

4.2 Measurements of Parrish et al[108]

In the work of Parrish et al the measurements of NO_2 photodissociation rates were made at a remote field station located in a forest clearing at the C-1 site of the Mountain Research Station of the University of Colorado at a surface level (3.05km asl) for low-albedo low-aerosol conditions. Clear-sky results were approximated with a simple analytic expression, which describes 95% of experimental data within ±7%, which is beleived to be the experimental precision. It had been reported, although that the latter estimate may be too optimistic (Blindauer et al[114]). We computed the $j(NO_2)$ surface values (accounting for 3.05 km elevation) for different surface types (with low spectral albedos) and atmospheric profiles with the *pressure-independent* refraction index of air and *zero* aerosol loading. The errors are presented in Fig.(8), where the naming scheme described in the previous section is used. Comparisons with the fitting expressions for surface values from Feister[110] and Dickerson et al[107] produced errors of the same magnitude.

4.3 Measurements of Dickerson et al[107]

As discussed in Ref.(107), the altitude dependence of the photolysis frequences of $j(O_3)$ and $j(NO_2)$ measured by different authors vary from no effect at all to a doubling by 5 km altitude. The authors of the cirted ref. had noted that in their measurements the photodissociation rate of NO_2 experienced no detectable change within estimated 9% experimental accuracy in the altitude range from 0.05 to 5 km. Variation of $j(NO_2)$ with height can be easily explained by the presence (or absence) of aerosols and effects of the surface albedo. In Fig.(9) the typical behaviour of $j(NO_2)$ with respect to height is plotted for clear-sky low-albedo high-sun conditions for the pressure-independent (labelled "R-000-A") and pressure-dependent (R-TPE-A and B for two values of surface albedo) refractive index of air. Obviously, in the pressure-dependent case the photodissociation rate of NO_2 experiences much smaller variations with altitude. Changes in surface albedo or slight increase of the aerosol loading in the near-surface layer almoust rigidly shifts the pressure-dependent curve. The same "forcing" applied to pressure-independent curve produces practically no change (not shown). Addition of scattering aerosols at higher altitudes makes the pressure-dependent curve look more like it's pressure-independent counterpart. At the same time the latter (when aerosols are added) doesn't much change it's shape. To "flatten" the

pressure-independent curve one must add a substantial amount of absorbing material. The values shown are near the upper limit of those measured in Ref.(107).

Weak temperature dependence reported in Ref.(107) could be attributed to the temperature dependence of the absorption crossection of NO_2. No temperature dependence of NO_2 quantum yield had yet been reported.

4.4 Comparison with photodissociation rates from European Chemistry Transport Model

The modelling system which has been developed in Langmann and Graf[115]) based on Ref.(72) contains a meteorological driver, an emission model and a chemistry-transport model CTM. In a modified version output from European area model REMO (Ref(83)) and/or HIRHAM (Ref(106)) models is used as meteorological input. Photodissociation rates are calculated at several selected heights for five latitude belts accounting for absorption of O_2 and O_3, Rayleigh scattering, clouds, aerosols and are further interpolated to the finer grid of the CTM (Ref(36)). Surface optical properties are also accounted for. Although this procedure is very fast, large errors introduced by coarse resolution were reported in Ref.(87). In our computations we used a wavelength grid with 78 nodes, pressure- and temperature-dependent refraction index of air and $O^3 \rightarrow {}^1D$ quantum yield parameterisation from Ref.(67)). Cloud parameterisations outlined in Section 3.5 (ECHAM-4 cloud scheme) were used together with the meteorological output from REMO model. Ozone, NO_2 and SO_2 concentrations in the troposphere were taken from CTM. Standard (Ref(42)) midlatitude summer values were substituted at levels higher than 200 mb. Aerosols were not accounted for. Surface parameters were determined according to the land use data from the CTM. Computations were performed for a set of hourly meteorological and concentrations data describing conditions over Europe in September 14-18, 1992, in a region from 7°W to 30°E latitude and from 30°N to 50°N longitude on a grid with 63 by 55 cells in the respective directions. We present here results of a comparison for September 16, at 12 GMT. CTM results were communicated to author by Dr. B.Langmann. Meteorological conditions did not change significantly during that day. Practically all northern Europe was covered with clouds, while at the Mediterranean region it was generally clear. Total (accounting for all levels) cloud cover at 12 GMT is given in the Fig.(10).

We start with the comparison of the column-averaged values. At the top panel of Fig.(11) the percent difference between CTM and the proposed method is shown for the $O^3 \rightarrow {}^1D$ reaction rate. The bottom panel of this figure gives the percent difference in bulk values of $j(NO_2)$. It can be seen that in cloudy regions (middle and northern Europe) the CTM model tends to underestimate both the bulk ozone destruction (by 10-40%) and production (by about 30%). In clear-sky cases (southern Europe) the ozone destruction is less by about 10-20%, but the bulk ozone production in the CTM (via NO_2 dissociation channel) is up to 20% larger.

The bulk values are determined mainly by the upper tropospheric and lower stratospheric levels, where the photodissociation rates are much higher than at or near the surface. Fig.(12) shows the percent deviation of surface values of ozone destruction rate (top panel) together with ozone production. While in clear-sky regions the behaviour of $j(O_3 \rightarrow {}^1D)$ is much like that for the bulk values (i.e. about 10-20% less), in cloudy regions the difference between two models becomes much more pronounced and site-dependent. Partly this reflects the difference in parameterisation of the clouds.

Contrary to the behaviour of the bulk values, surface ozone production rate ($j(NO_2)$) as predicted by the CTM is uniformly smaller than in the advocated method both in clear (with exeption of

south-western Europe) and cloudy regions, the difference being more pronounced in the latter case. Also, in cloudy regions the values produced by the models being compared are sometimes in complete disarray. We attribute that to the crudeness of the CTM radiation code.

Next two figures illustrate the altitude dependence of the photodissociation rates. Figs.(13) shows the rate of $O^3 \rightarrow {}^1D$ and NO_2 dissociation at model level 4 (approximately 930 mbar), Figs.(14) - at model level 8 (approximately 750 mbar). CTM predicts ozone destruction rate to be more or less uniformly smaller than that for the method being presented, especially in the cloudy regions. The behaviour of $j(NO_2)$is different. While in the cloudy regions it is CTM gives smaller values, in the southern/south-western part of Europe this model significantly overestimates the rate of $j(NO_2)$ reaction. The discrepancy between two models decreases with height.

In general, bulk values produced by both models are in good qualitative agreement. This is not surprising, because they are dominated by values in the higher atmosphere. Let's qualitatively separate the photochemical reactions in "absorption-dominated", like $O^3 \rightarrow {}^1D$, and "scattering-dominated", like NO_2 dissociation. Then, for clear-sky low-illumination conditions the CTM code generally gives lower values for the "absorption-dominated" reaction rates and higher for "scattering-dominated" compared to the advocated method. When the incoming radiation grows, the discrepancy in "absorption-dominated" reaction rates stays approximately the same while the discrepancy in the efficiency of the "scattering-dominated" reactions increases. The efficiency of "absorption-dominated" reactions is determined primarily by the absorption in the lower stratosphere and bulk amount of ozone. Thus, for clear-sky high-sun conditions one might expect good agreement between two models. Nevertheless, scatterers, such as clouds or aerosols, may significantly affect the rate of these reactions. At the same time, the NO_2 dissociation is driven almost entirely by scattered radiation. When scatterers are present, the CTM model quiet often produces unrealistic values for dissociation rates of interest. This is clearly seen in Figs.(12-14) where the CTM fails to reproduce the enhancement of photodissociation due to clouds in the Mediterranean region (black spots in Figs.(12-14) represent discrepancies larger than 100%).

Actual distributions of the reaction rates at the surface are presented in Figs.(15-16), where the top panel represents the CTM values and the bottom one- values from the present method. Fig.(15) shows the ozone destruction rate ($O^3 \rightarrow {}^1D$ channel), Fig.(16) the rate of dissociation of NO_2..

Implications of these results for the tropospheric chemistry will be discussed in a future work.

5. Uncertainties and error analysis

In the papers devoted to the sensitivity studies and error analysis it is often assumed that the numerical and physical issues may be separated. Quite often, a statment is made like "it had been shown that absolute accuracy of the numerical method with this and that set of parameters is ..." (de F.Forster[116], Weihs and Webb[117118], Ref(2) etc) and further all the discrepancies among the measured and calculated quantities are attributed to the uncertainties in the coefficients or inadequacy of parameterisations used. Unfortunately, this assumption is justified only for the clear sky computations (with certain precautions and limitations,- for example, solar zenith angle should exceed some specific value for any given angular resolution). The main source of trouble is the fixed spatial grid. Ideally, for each computation, the grid in the spatial (here, vertical) coordinate should be selected based on the actual distribution of absorbers and scatterers with due regard to their variation along the optical path. For example, insertion of even moderate amounts of scattering aerosol over low-albedo surface leads, in the vicinity of the latter, to pronounced changes in the vertical structure of the intensity field and it's moments, so that the introduction of additional

layers in order to resolve these changes becomes vitally important. When the cloud boundary falls between layer boundaries, the errors may become intolerably large. Another serious problem is the homogeneous layers assumption. The majority of the plane-parallel radiative transfer solvers (this one is no exeption) postulate a piecewise-constant distribution of absorbers. This assumption had become such common, that this source of errors is never even mentioned. It may be argued that these errors tend to zero when the grid is refined, but normally we are dealing with very crude approximations. In general, the problem of determining the equivalent piecewise-constant distribution of absorbers is not at all trivial. To find this distribution we have to solve the adjoint equation of radiation transfer several times (for discussion and algorithms see Ref.(9)), which is not easier than the solution of the radiative transfer equation itself. The above discussion refers primarily to the aerosols and clouds. But it applies also to gases especially when the absorption crossections of the latter exhibit temperature or pressure dependence. To certain extent, some of these problems may be battled with the introduction of higher order methods and adaptive vertical gridding, but, in general, because of the high variability of atmospheric conditions, computationally efficient remedies are not known. As follows from this discussion it is very hard to give error estimates for the general case. It is relatively safe to assume, for the time being, that numerical errors will not be less than those estimated in the testing above. (Author is fully aware of the potential of physical "tuning",- see, for example, sections 4.1 or 4.2 of this report). We proceed now to the brief review of the physical error analysis made in other studies.

In the work of Schwander et al[119] the uncertainties in the modelled spectral UV-irradiances are analysed for the cloud-free conditions with respect to the limited accuracy and availability of input data. They assume that internal parameters of the radiation model (absorption crossections, solar flux etc) are error-free and estimate the uncertainties in the spectral UV-irradiance to be within 10-50% and for spectral integrals (photodissociation rates, heating rate) within 10-15% for the situations when retreived "bulk" properties (total ozone amount, column aerosol optical thickness etc) are used to scale the standard atmospheric profiles. The authors express the opinion that when actually measured values are substituted, the uncertainties reduce to values between 2 and 6%. With the discussion of errors in aerosol retrieval algorithms (Ref.(77)), this estimate seems to be too optimistic.

Two papers (Ref.(116)) and de F.Forster et al[120] are devoted to the development of the radiative transfer model suitable for modeling ultraviolet radiation at the Earth's surface. In this rather detailed study, the issues related to the numerical accuracy, uncertainty in internal parameters (absorption cross-sections and the like) and input data are addressed. Results of extensive sensitivity studies are provided and, in the second paper, the comparison with observations is made. The physical model is based on a lookup table of standard profiles and aerosol and cloud types wich are shifted according to the bulk amounts obtained from other sources. Three types of clouds are present with their boundaries confined in certain height ranges. This is exactly an approach which had been critisized in Ref.(119). Ground albedo adopted in these comparisons seem to be too high (0.1 at 280 *nm*, linearly growing towards larger wavelengths). The following citation from Ref.(120, page 2433) clarifies the approach: "With careful tweaking of the model wavelengths, the ratio's (computed to measured, V.P) noisiness and short-wave differences could be reduced". With "careful tweaking" the reported errors in clear conditions were found to be around 10%.

Another extensive study of accuracy of spectral UV model calculations is that given by Refs.(117,118). In this work a numerical model was assumed to be absolutely accurate and only uncertainties in the input parameters were estimated in the first part of the paper (Ref.(117)). Assuming that there are no errors in vertical temperature and ozone profile, and doing calculations

for a range of values of the zenith angle, total ozone content, albedos, and aerosol optical depths, these authors arrived to the following estimates. At the wavelength 305 *nm* the overall accuracy varied from ±16% (15.99 in the cited ref) for overhead sun to ±26% for lower elevations. At 380 *nm* estimates were better and varied from ±4 to ±15%. In the second part of the paper (Ref.(118)) the authors show how the uncertainty of the input parameters offers several degrees of freedom to match the observations (as in Ref.(120))

To summarise, errors due to uncertainty of atmospheric parameters for the majority of the clear-sky atmospheric conditions and practical angular and vertical resolutions are beleived to be no less than 10% with a relatively safe estimate about 1.5-2 times larger. In this estimate problems with partial cloud cover are not accounted for, as no direct evidence was found in the literature. (Side illumination effects and shadowing were estimated in Ref.(89). The results of comparison of a three-dimensional Monte-Carlo simulation with δ-two stream approximation lead the author of Ref.(89,p.269) to the conclusion that "on scales, where (radiative) energy exchange between different grid columns becomes important, any scheme which considers each column in isolation will fail").

Absorption crossections of O_3 and NO_2 , are reportedly determined with accuracy better than 5% (Refs.(53,66,67,70)). Combined uncertainties in quantum yields and crossections as estimated in Ref.(67) are 30% for $O_3 \rightarrow {}^1D$ reaction in the troposhere-relevant wavelength range (see also Fig.(5), where two formulas for the quantum yield are compared), 20% for NO_2, 50% for NO_3 , and for other species reported uncertainties are of the same magnitude at worst. When retreived optical properties of aerosols are analysed using conventional Mie theory, the errors can easily exceed 100% (Ref.(77)). It is questionable whether one may reliably predict optical properties of clouds neglecting the effects of aerosol pollution (Ref.(96)). There is continuing research in the determination of the optical parameters of various surfaces. At the same time the effects of non-lambertian surface reflectivity are still poorly understood (see Ref.(100), Barichello et al[121], Godsalve[122], Settle[123] and for discussion of snow optical properties Leroux et al[124], Steffen[125], Aoki et al[126], to mention only some recent publications). Nitrogen dioxide is an important absorber and should be included in the radiative transfer computations, it influences also the $O(^3P)$ ozone destruction channel. Finally, the introduction of additional gaseous absorbers in the radiative transfer which, normally, are present only in trace concentrations (NO_3, CH_2O etc) may change the relevant photodissociation rates at most by 2-5%. This upper bound estimate is based on the variability of the chemical composition of the atmosphere as proposed by the CTM concentrations data (B. Langmann, personal communication) and numerical experiments (not shown) performed for the standard atmospheric profiles of O_3 and NO_2 and various aerosol loadings.

Regarding the estimates of errors due to uncertainties in atmospheric parameters (Refs.(116-120)), one should note that the assumption of the absolute numerical accuracy of the method is rather questionable even for the clear-sky cases. As results from sections 2.4.1 and 2.4.3 indicate, for the practical resolutions both in vertical and angular coordinates (those that were used in the above cited refs), the average (wrto altitude) error in frequency integrated actinic flux is about 2%. The maximum (again with respect to altitude) errors for these cases were several times larger, so they compare well with or exceed the estimated uncertainties.

6. Summary

In this report a set of efficient algorithms for the solution of the plane-parallel radiative transfer problems had been described. Although only tests with a beam source were presented, the algorithms outlined are equally well suited for computations in the terrestrial portion of the

spectrum. While maintaining the same level of accuracy as other established solvers, the proposed algorithms are 60-100 times faster either in scalar or vector mode even without compiler- or hardware-specific optimisations. A comprehensive package of FORTRAN subroutines suitable for massive computations of radiative fluxes and photolytic rates has been designed and implemented. It's performance is at the level of the fastest solvers reported. It's description and user manuals for various components are described in the second part of this report.

Numerical experiments have confirmed (Refs.(2,6,7)) that a rather large number of streams/moments is needed for the accurate representation of the actinic flux. The very stretched phase functions inherent to problems in atmospheric radiative transfer demand high angular resolution. At the same time, errors introduced by violation of the step size constraint are relatively smaller and may be effectively dealt with by insertion of additional levels or implementation of higher order schemes (Refs.(3,23)). These schemes will also make it possible to reduce the number of levels in the vertical coordinate to the essential minimum, defined by the distribution of non-gaseous absorbers, i.e., clouds and aerosols.

It was shown that for the fluxes and heating rate computations the combination of finite-difference discrete ordinates with the Legendre expansion of the phase function results in a nearly optimal algorithm in terms of accuracy and performance. At the same time the use of Legendre polynomial expansions of the phase function in the calculations of intensity may give incorrect results in the azimuthal directions other than that of the incident beam. These errors grow when the phase function becomes more stretched. The proposed remedy is the use of the fully discrete approximation in the quadrature form with the composite quadrature rule like that used in Ref.(19) for the zenith angle and uniform discretisation in azimuth.

The construction of a numerical method suitable for massive computations cannot be separated from the choice of an "optimal" set of wavelengths together with development of the interpolation and averaging procedures. In this study we used the local basis approach for the construction of the integration rules for photodissociation rates. More efficient integration procedures will be described in a separate paper.

The pessimistic error estimates given in section 5 refer primarily to the combination of variability of parameters describing the atmospheric state and fixed vertical grid. For the computations like those presented in section 4.4, when tuning is not possible and meteorological variability of parameters comes into play, these errors are definitely several times larger than those resulting from numerical scheme and inaccuracies in crossections. Errors introduced by meteorological driver, by the "capping" procedure (that is, the prescription of absorber amounts at levels where data is not available, say, higher than 200 mbar) and rather crude surface albedo parameterisations may be, in the worst case, of the same magnitude. That is because the reaction rates (especially 'absorption-dominated") are rather sensitive even to moderate variations in bulk amounts of absorbers (see also Ref.(87)). Redisitribution of ozone in the lower stratosphere (with the same total column amount) also leads to pronounced changes in the reaction rates. Obviously, the improved characterisation of the absorbers profiles will significantly increase the quality of modelling.

The largest gain in accuracy of photochemical computations can be achieved through better characterisation of the atmospheric aerosols , clouds and their interaction. As can be inferred from Ref.(96), the optical properties of mixtures are highly nonlinear functions of their composition and require special accessment. At the same time, the introduction of the improved retrieval procedures may significantly improve the quality of the site-based computations. A very promising and mathematically sound approach to the on-line assimilation of the observational data in the

comprehensive tropospheric gas phase chemical model was described in Elbern et al[127] . The adjoint variational formulation in this approach is naturally underlies the retrieval procedures in radiative transfer and could be effectively implemented for the latter, giving, at the same time the possibility to detrmine adequate vertical grid.

Contrary to rather well established crossection values for most gases, there is some unclarity regarding the refractive index of clean air. Numerical experiments show that the pressure and temperature dependence of the refractive index of air (as given by Ref.(45), see sections 3.2, 4.1, 4.3) is crucially important for the modelling of the photochemical and radiative processes in the troposphere. Therefore the direct measurements of the Rayleigh scattering coefficient for various temperature and pressure conditions are required.

7. Acknowledgements

This work had been done during the author's stay in Max-Planck Institute of Meteorology, in Hamburg, Germany. I am pleased to express my gratitude to Hans F. Graf, Ingo Kirschner, Judith Perlwitz, Baerbel Langmann, Michael Herzog and Iris Engelmann for support and help provided in the course of this work. It is a pleasant duty to express gratitude to Dr. J.Orphal from the University of Bremen for finding the possibility to share the absorption crossection data prior to publication (Refs.(70,71))

8. Figures

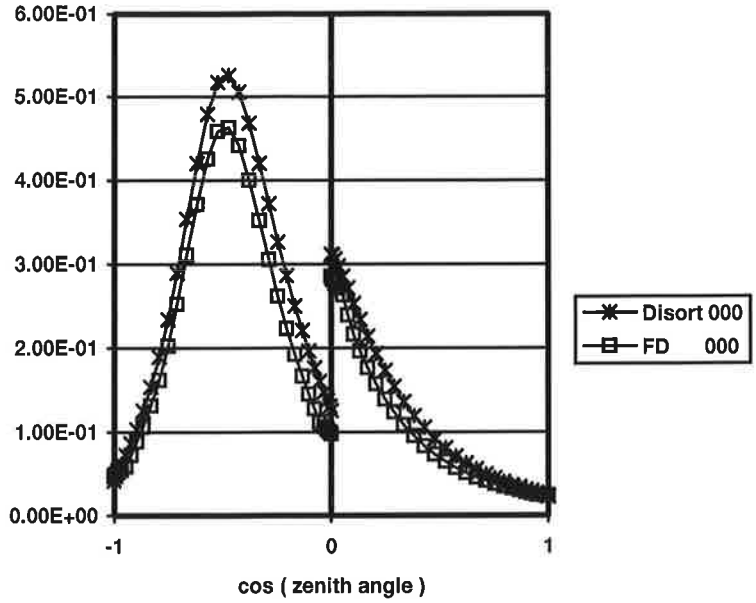

Figure 1. Transmitted (left panel) and reflected (right) irradiance at $\Delta\varphi=0°$

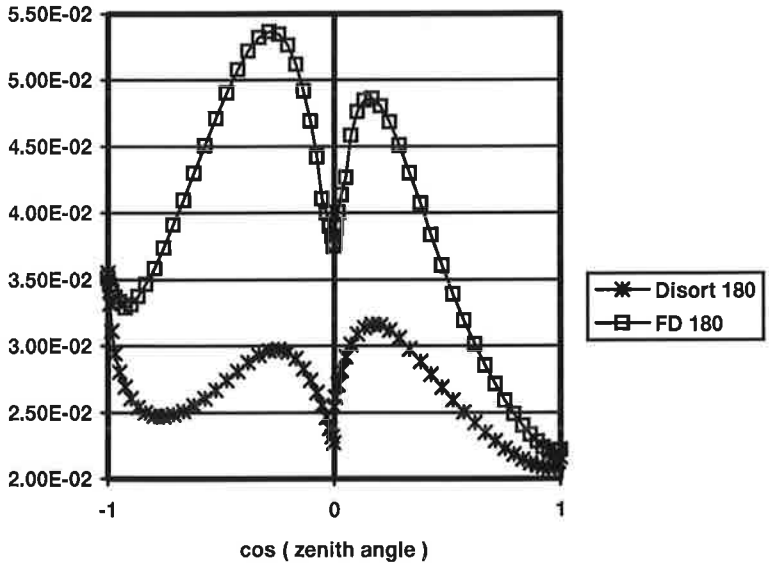

Figure 2. Transmitted (left panel) and reflected (right) irradiance at $\Delta\varphi=180°$

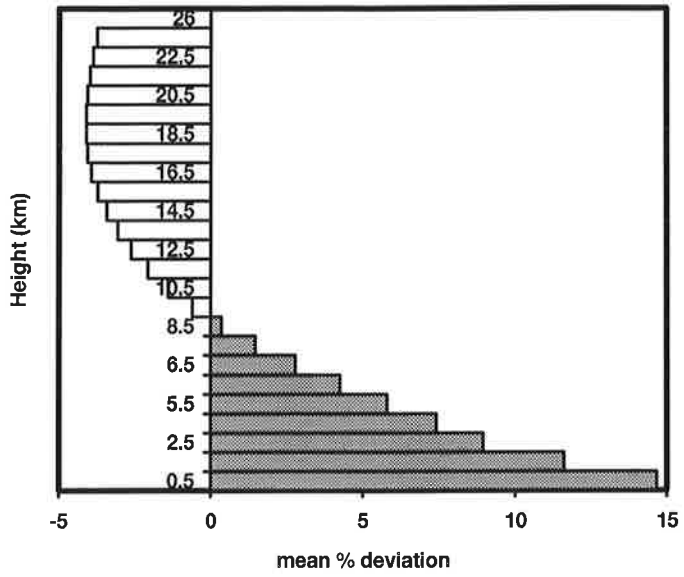

Figure 3. Pressure correction effect on heating rates

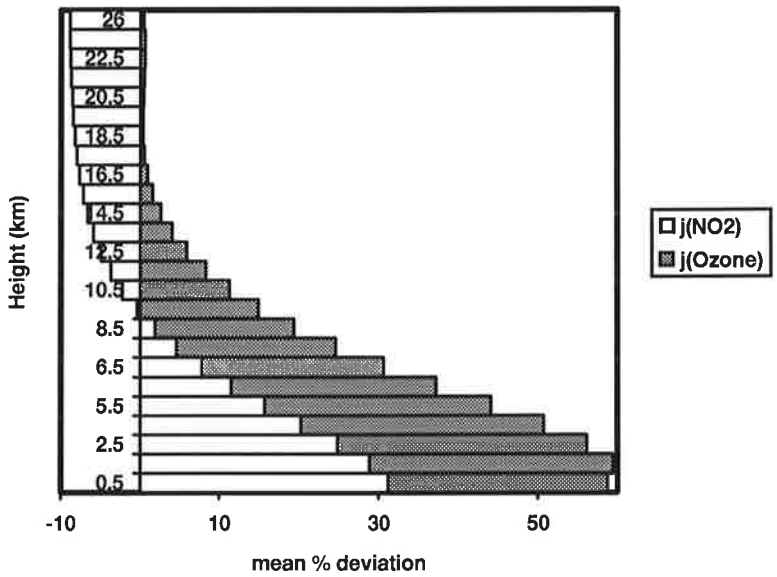

Figure 4. Pressure correction effect on $j(O_3 \rightarrow {}^1D)$ and $j(NO_2)$

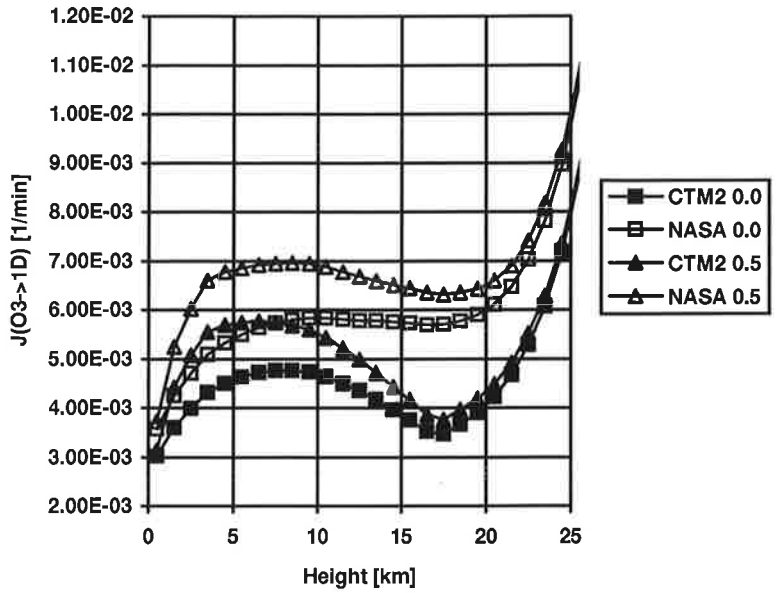

Figure 5. Comparison of formulae for $O_3 \rightarrow {}^1D$ quantum yield

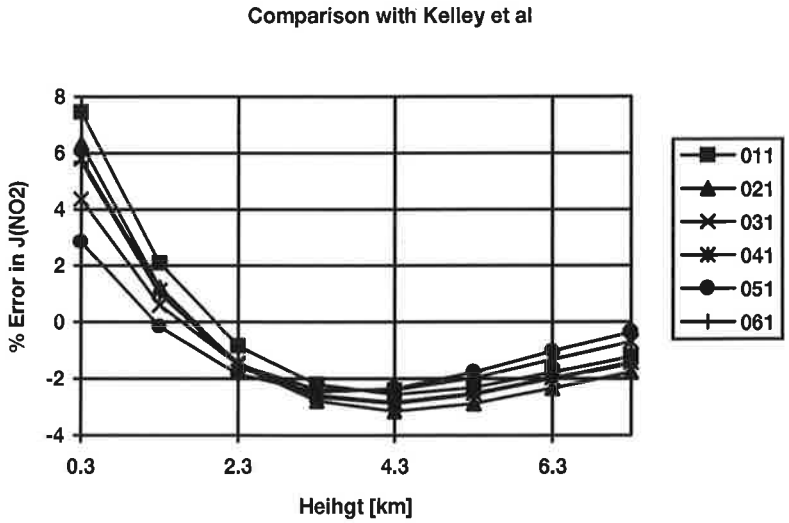

Figure 6. Clear case, non-TPE refraction, varying ozone profile

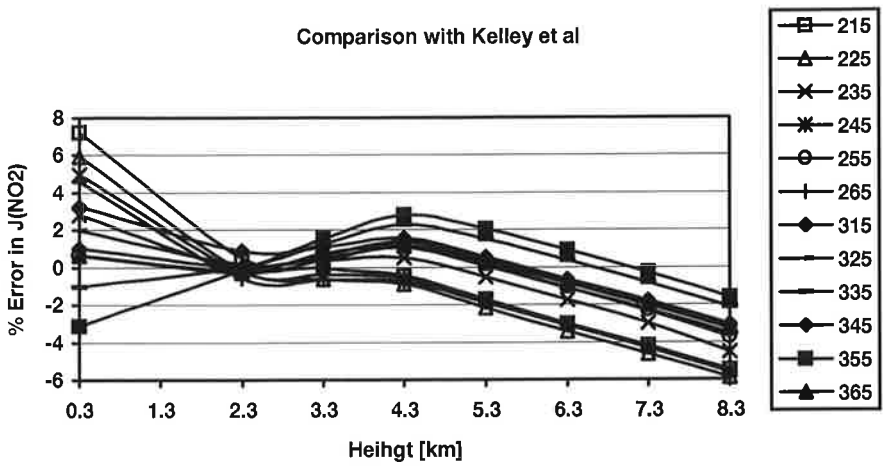

Figure 7. TPE-dependent refractive index, 2 aerosol cases, varying ozone profile

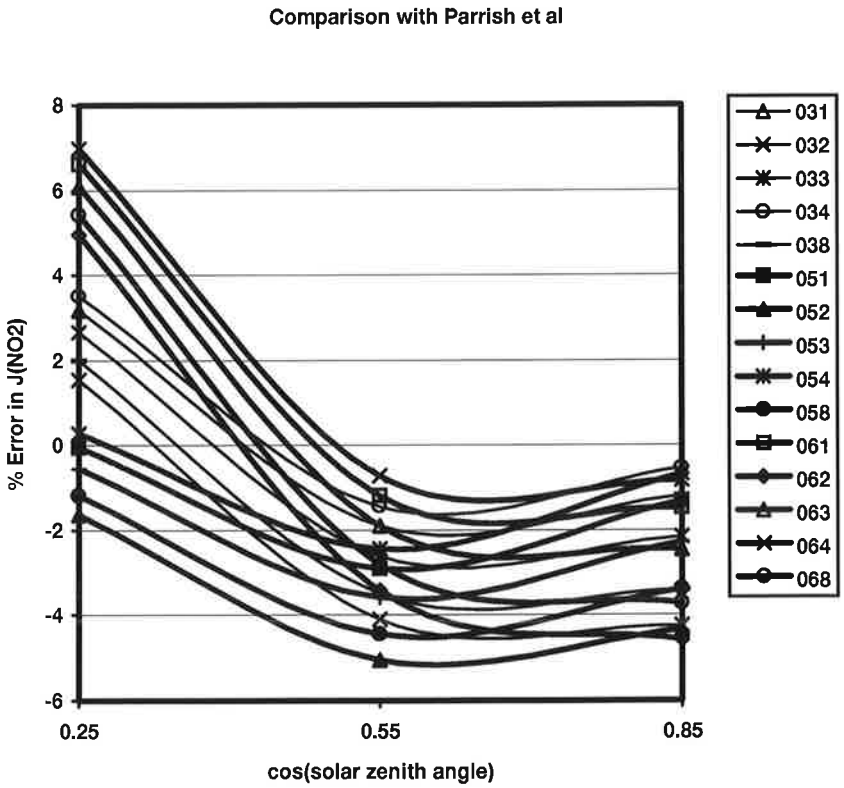

Figure 8. Deviations for varying ozone profile and surface type

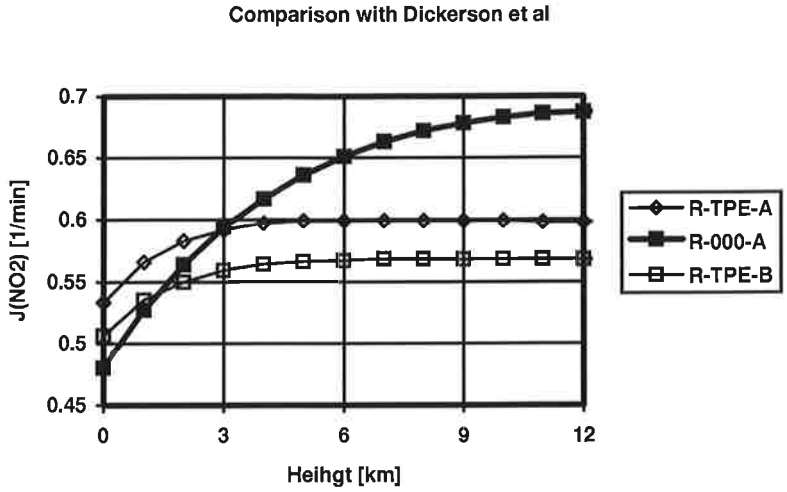

Figure 9. Altitude dependence of $j(NO_2)$

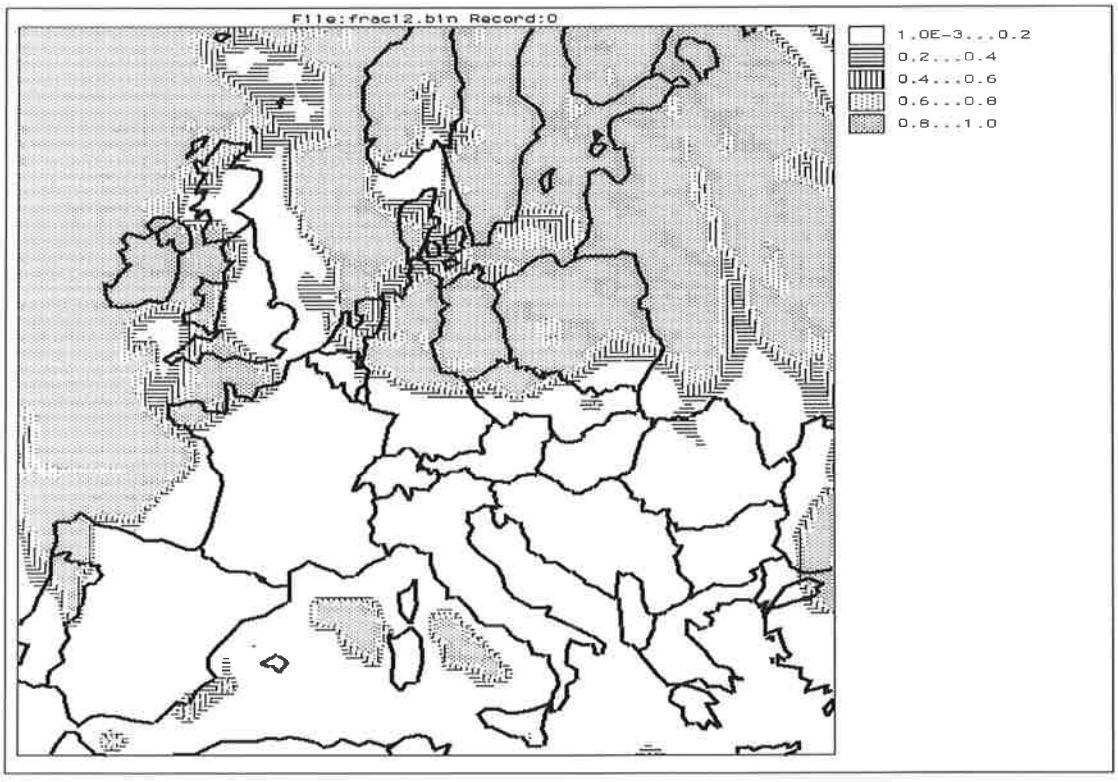

Figure 10. Cloudiness 1200 GMT

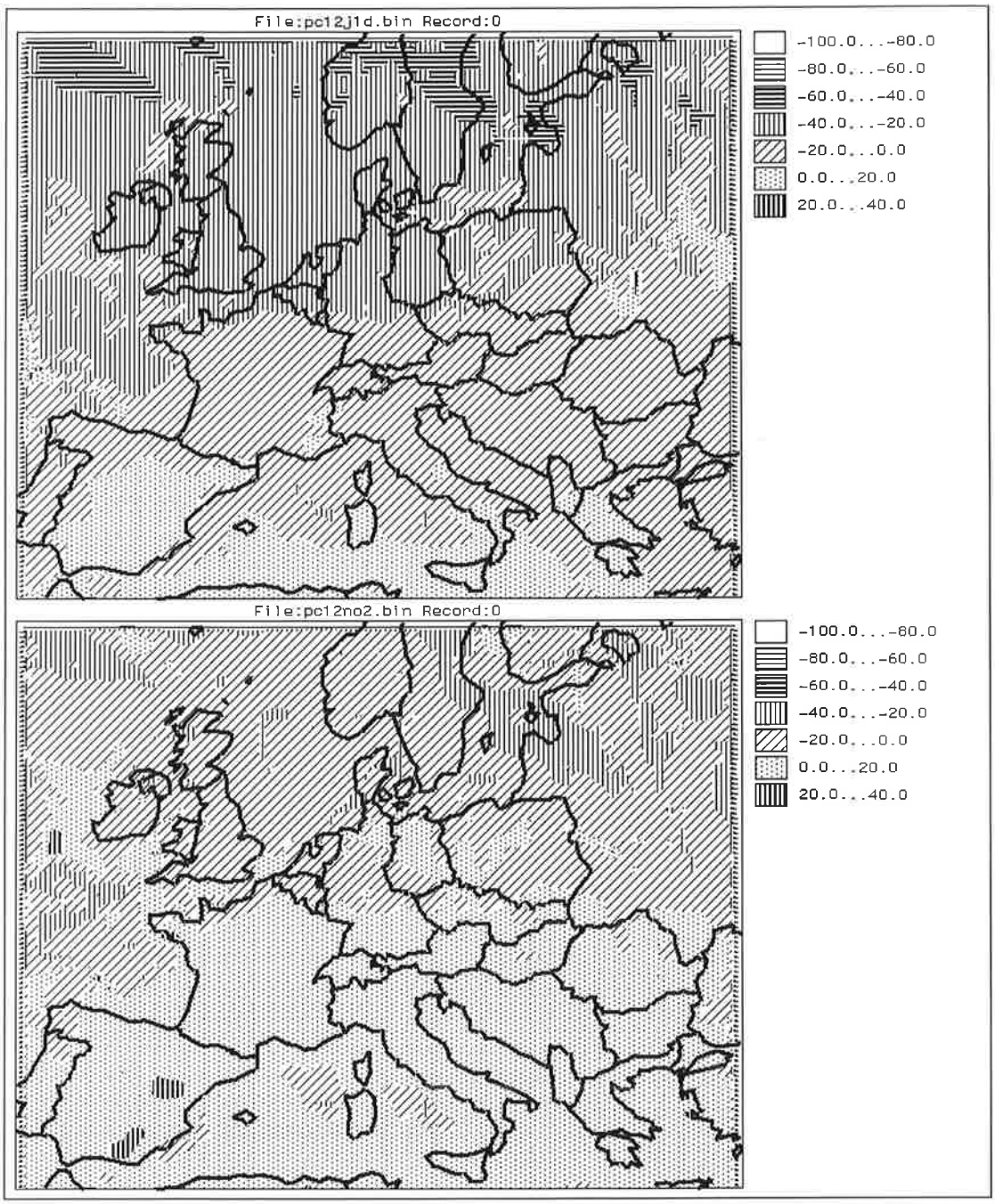

Figure 11. % difference in bulk values of $j(O_3 \rightarrow {}^1D)$ (top panel) and $j(NO_2)$ (bottom)

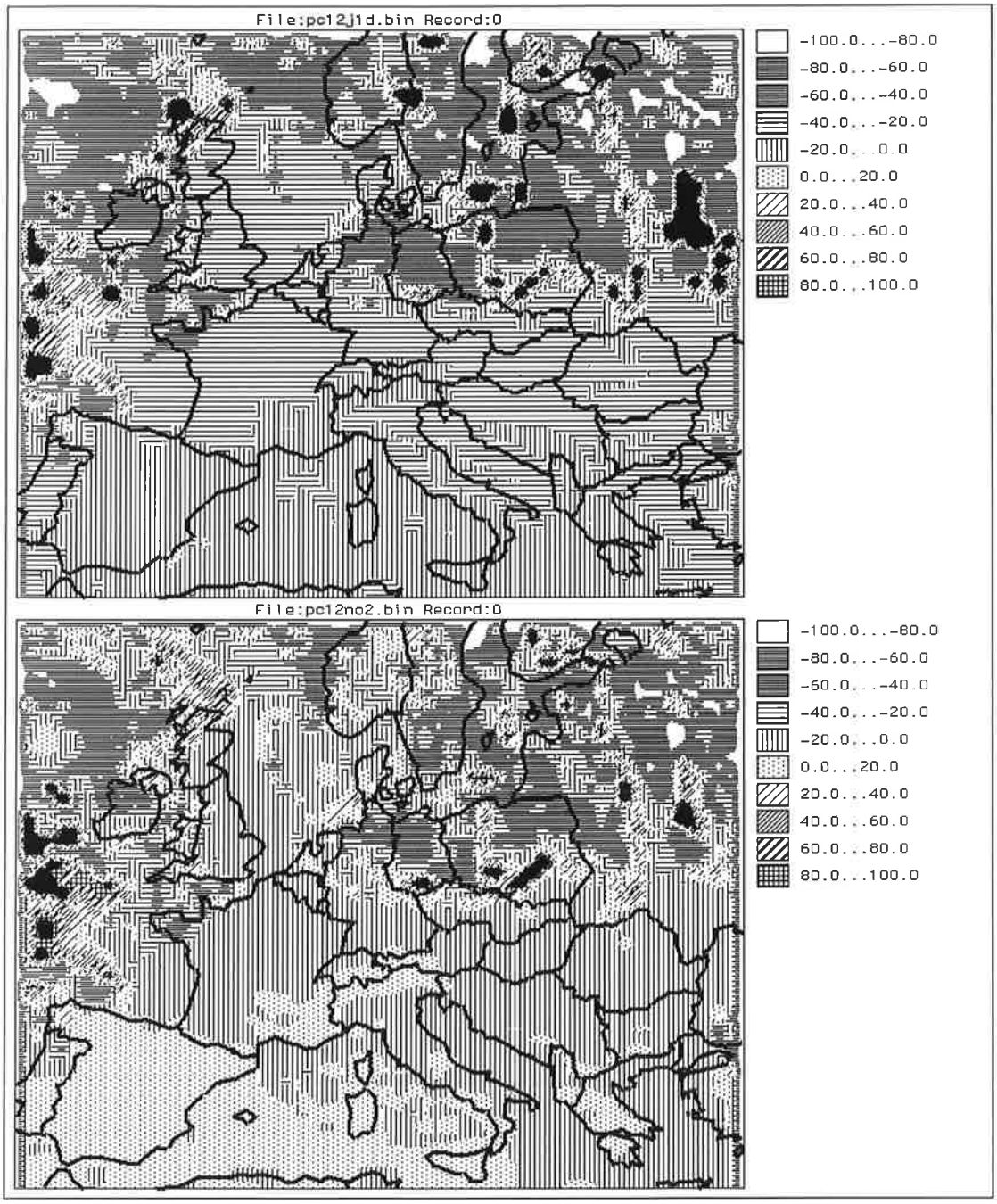

Figure 12. % difference in surface values of $j(O_3 \rightarrow {}^1D)$ (top panel) and $j(NO_2)$ (bottom)

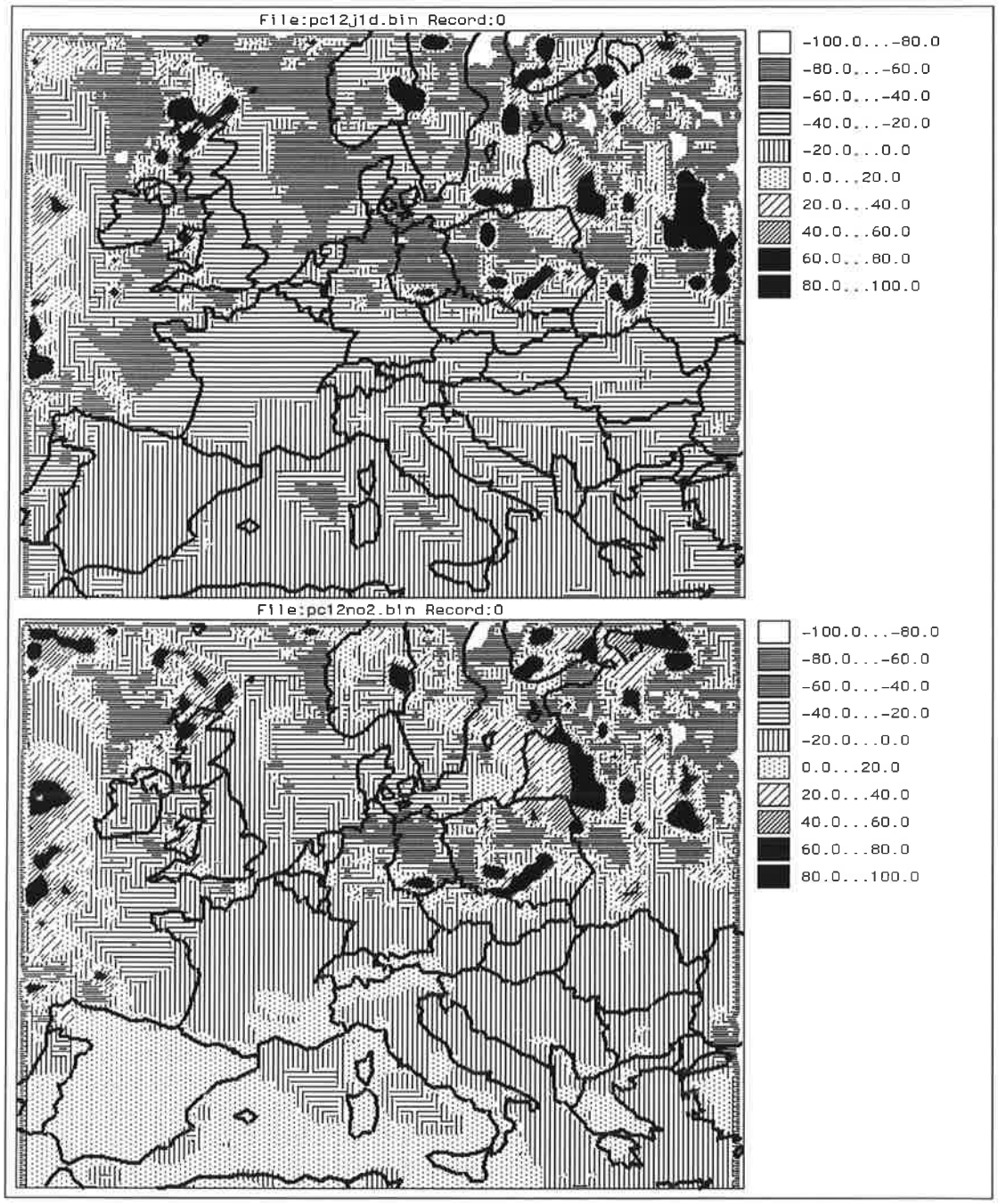

Figure 13. % difference in values of $j(O_3 \rightarrow {}^1D)$ (top panel) and $j(NO_2)$ (bottom) at model level 4

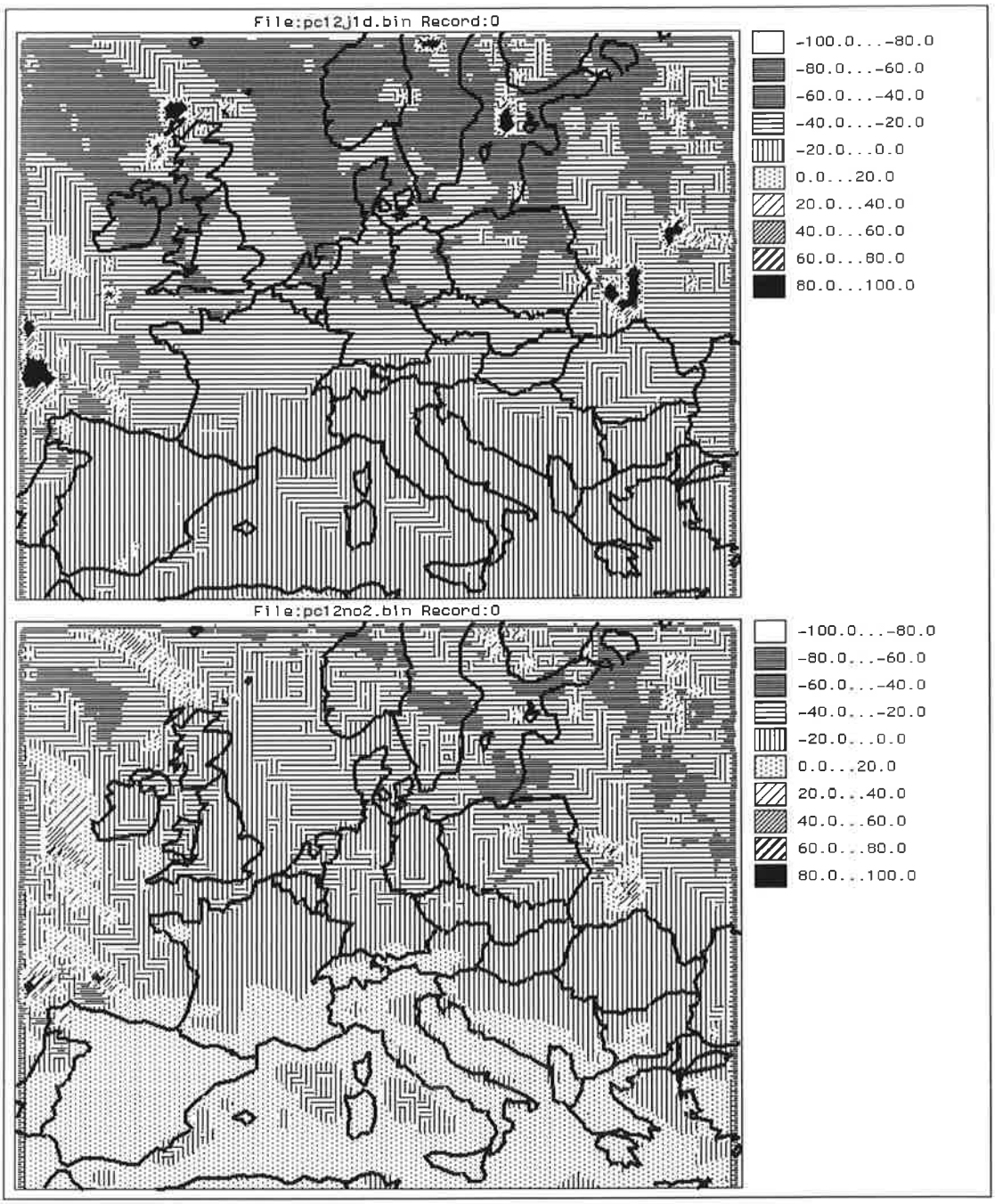

Figure 14. % difference in values of $j(O_3 \rightarrow {}^1D)$ (top panel) and $j(NO_2)$ (bottom) at model level 8

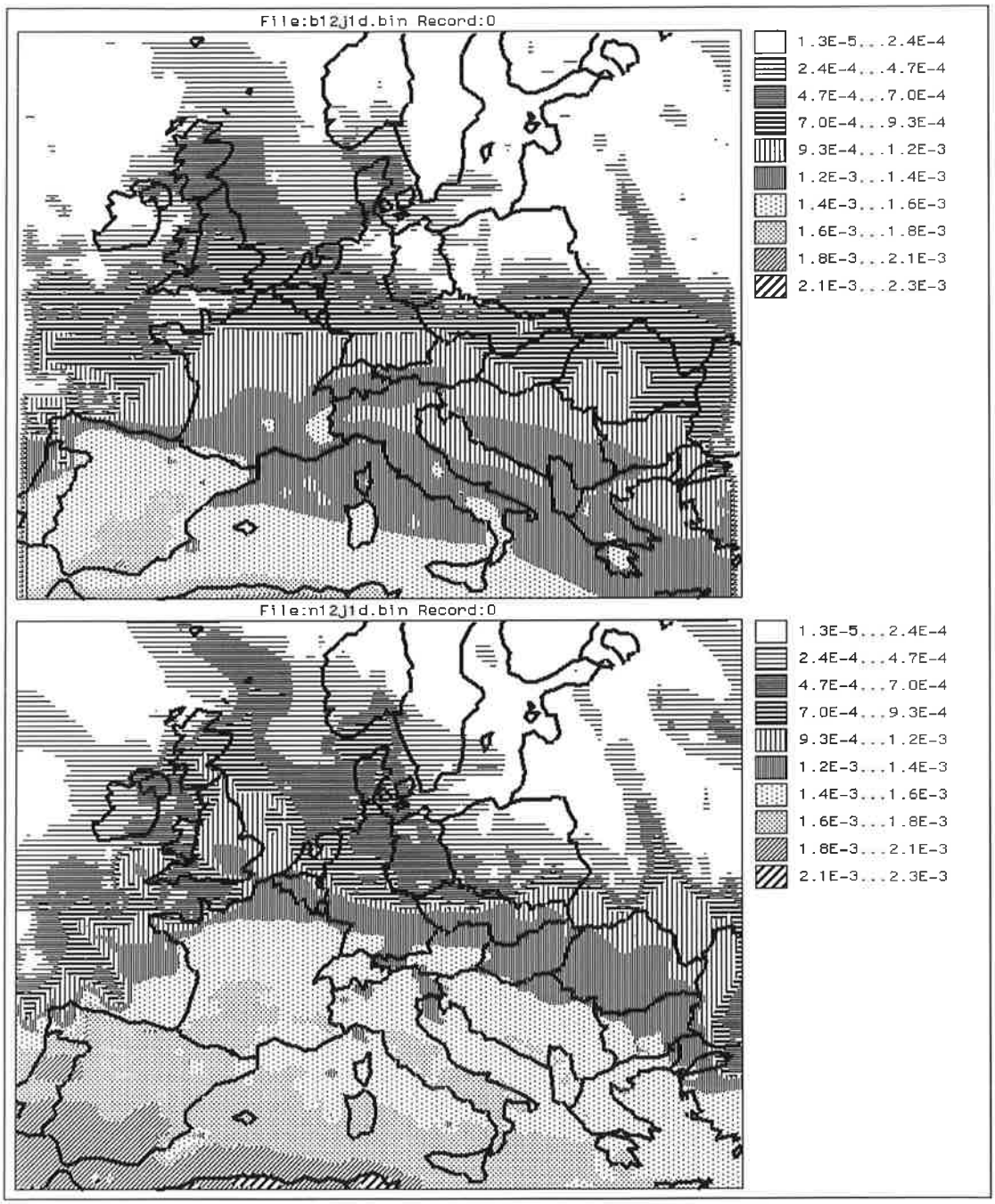

Figure 15. Surface values of $j(O_3 \rightarrow {}^1D)$ from CTM (top panel) and new (bottom) models

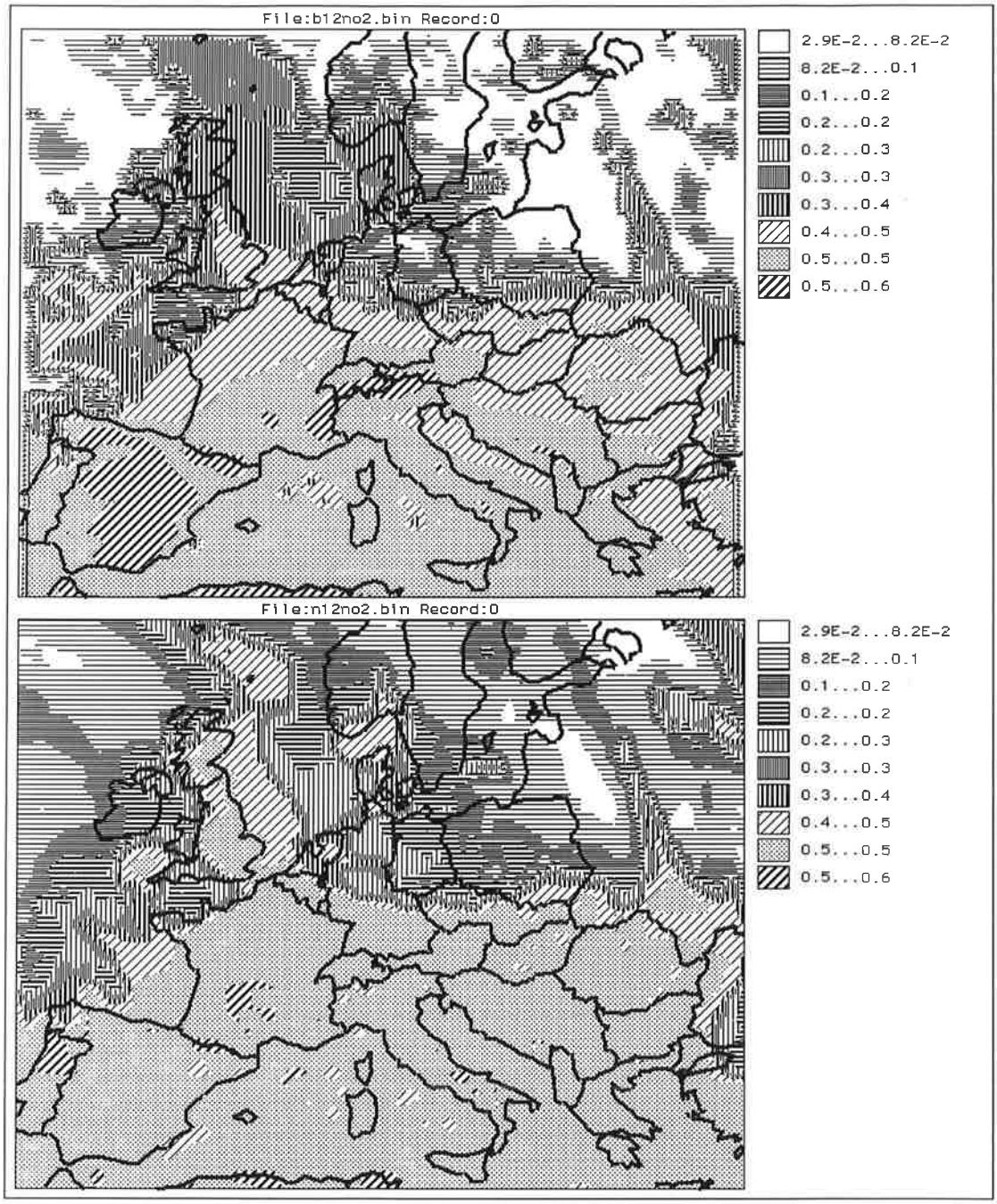

Figure 16.Surface values of $j(NO_2)$ from CTM (top panel) and new (bottom) models

9. Literature

[1] Acquista C., F.House, J.Jafolla, N-Stream Approximations to Radiative Transfer, *JAS*, **38**, 1446, (1981).

[2] Ruggaber A., R.Dlugi, T.Nakajima, Modelling Radiation Quantities and Photolysis Frequencies in the Troposphere, *J.Atmos.Chem.*, **18**, 171, (1994).

[3] Marchuk G.M., V.I.Lebedev, *Numerical methods in neutron transport theory*, Atomizdat, Moscow (1971), in russian.

[4] Stamnes K., R.A.Swanson, A New Look at the Discrete Ordinate Method for Radiative Transfer Calculations in Anisotropically Scattering Atmospheres, *JAS*, **38**, 387,(1981).

[5] Nakajima T., M.Tanaka, Matrix Formulations for the Transfer of Solar Radiation in a Plane-parallel Scattering Atmosphere, *JQSRT*, 35, **1**, (1986).

[6] Rozanov V.V., D.Diebel, R.J.D.Spurr, J.P.Burrows, GOMETRAN: A radiative transfer model for the satellite project GOME, the plane-parallel version, *JGR*, **102**, 16683-16695, (1997)

[7] Moncet J.L., S.A.Clough, Accelerated monochromatic radiative transfer for scattering atmospheres: Application of a new model to spectral radiance observations, *JGR*, **102** (D18), 21853-21866,(1997).

[8] Samarsii A.A.,*Theory of difference schemes*,Moscow,Nauka.

[9] Marchuk G.M.,*Methods of numerical mathematics*, 2nd edition, Springer Series "Applications of Mathematics", Springer, 1982.

[10] Fedorenko R.P, *Introduction to Computational physics*, "Nauka",Moscow, (1994), in russian.

[11] Lenoble J., *Radiative transfer in scattering and absorbing atmospheres: standard computational procedures*,A.Deepak Publishing,Hampton,Virginia USA,(1985).

[12] Kurosu T.,V.V.Rozanov,J.P.Burrows, Parameterization schemes for terresrial water clouds in the radiative transfer model GOMETRAN, *JGR*,**102** (D18), 21809-21823,(1997).

[13] Chandrasekhar S., *Radiative transfer*, Oxford Univ. Press, London (1950), and Dover, New York (1960).

[14] Zdunkowski W.G.,R.M. Welch, G. Korb, *Beitr. Phys. Atmos.*, 53(2),147-166,(1980).

[15] Li J.,V.Ramaswamy, Four-Stream Spherical Harmonics Expansion Approximation for Solar Radiative Transfer, *JAS*, **53**, 1174-1186,(1996)

[16] Kylling A., Stamnes K., Tsay S.-C., A Reliable and Efficient Two-Stream Algorithm for Spherical Radiative Transfer: Documentation of Accuracy in Realistic Layered Media, *J. Atmos. Chem.*, **21**, 115-150, 1995.

[17] Sykes J.B., Approximate Integration of the Equation of Transfer, *Mon. Not. Roy. Astron. Soc.*, **111**, 377,(1951).

[18] Schuster A., *Astrophys. J.*, **21**, 1, (1905).
[19] Fricke C.L., The Phase-integral Method for Radiative Transfer Problems With Highly-peaked Phase Functions, *JQSRT*, **20**, 429, (1979).
[20] Kisselev V.B.,L.Roberti,G.Perona, An application of the finite element method to the solution of the radiative transfer equation, *JQSRT*,**51**,603-614,(1994)
[21] Gear G.W., *Numerical Initial Value Problems in ODE's*, Prentice Hall, (1971).
[22] Hall G., Watt J.M., (eds.), *Modern numerical methods for ODE's*. Clarendon Press, Oxford, (1976).
[23] Hairer E., G.Wanner, *Solving Ordinary Differential Equations, Parts I and II*, Springer Series in Computational Mathemtics, Vol.14, Springer Verlag,second edition, (1996).
[24] Butcher J.C., Ortogonal polynomials
[25] Kalitkin N.N., Kuzmina L.V., *Integration of the systems of stiff ordinary differential equations*, Institute of Applied Mathematics of the USSR Academy of Sciences, preprint N80, (1981), in russian.
[26] Vladimirov V.S., *Mathematical problems in one-velocity theory of particle transport*. Mathematical Institute of the USSR Academy of Sciences, (1961), in russian.
[27] Marshak R., Theory of the Slowing Down of Neutrons by Elastic Collision with Atomic Nuclei, *Phys. Rev.*, **71**, 443, (1947).
[28] Gryn V.I., On the Variational Principles in Radiative Transfer, *J. of Comput. Math. and Math. Phys.*,edition of the USSR Academy of Sciences, **1**, 5, (1984), in russian.
[29] Davis P.J, P. Rabinovitz, *Methods of Numerical Integration*, 2nd edition, Academic Press, 1984.
[30] Key J.,*Streamer User's Guide*, Technical Report 96-01, Departament of Geography, Boston University, 85 pp
[31] Wiscombe W.J., The delta-M Method: Rapid Yet Accurate Radiative Flux Calculations For Strongly Asymmetric Phase Functions, *JAS*, **34**, 1408, (1977).
[32] Kantorovich L.V.and V.I.Krylov, *Approximate methods of higher analysis*, Moscow, Fizmatgiz, (1962), in russian. There is a German translation L.W. Kantorowitsch, W.I. Krylov, Naherungsmethoden der Hoherenanalysis, Deutscher Verlag der Wissenschaftten, Berlin, 1956.
[33] Landgraf J., Crutzen P.J., Bruhl C., Efficient 'on-line' calculations of photolysis and heating rates, in the proceedings of IRS'96:Current Problems in Atmospheric Radiation, Smith and Stamnes (eds.), A.Deepak, (1997).
[34] Anderson G.P., S.A.Clough, F.X.Kneizys, J.H.Chetwynd, E.P.Shettle, *AFGL Atmospheric constituents profiles (0-120km)*,AFGL-TR-86-0110,(1986)

[35] d'Almeida G.,G.P.Koepke,E.Shettle, *Atmospheric aerosols global climatology and radiative characteristics*, A.Deepak, Hampton,Va.,(1991).
[36] Madronich S., Photodissociation in the atmosphere, 1, Actinic flux and the effects of ground reflection and clouds, *JGR*, **92**(D8), 9740, (1987).
[37] de Boor, C., *A Practical Guide to Splines*, Springer, 1982
[38] Gautschi W., Algorithm 726: ORTHPOL- A Package of Routines for Generating Orthogonal Polynomials and Gauss-Type Quadrature Rules, *ACM TOMS*, **20**, N1, 21-62,(1994).
[39] Vladimirov V.S., *Numerical solution of the kinetic equation on the sphere*, in "Computational Mathematics", N3, edition of USSR Academy of Sciences, Moscow (1958), in russian
[40] Kurucz R.L., *The Solar Irradiance by Computation*, Proc. 17th Annual Review Conference on Atmospheric Transmission Models, Geophysics Directorate/Phillips Laboratory,(1994).
[41] Berk A., Bernstein L.S., Robwertson D.C., *"MODTRAN: A Moderate Resolution Model for Lowtran 7"*, GL-TR-89-0122, (1989)
[42] Kneizys F.X., L.W. Abreu, G.P. Anderson, J.H. Chetwynd, E.P. Shettle, A. Berk, L.S. Bernstein, D.C. Robertson, P.Acharya, L.S. Rothman, J.E.A. Selby, W.O. Gallery, S.A. Clough, *The MODTRAN 2/3 Report and LOWTRAN 7 MODEL*. (1996)
[43] Edlen B., The Dispersion of Standard Air, *J. Opt. Soc. Am.*, **43**,N5,339-344,(1953)
[44] Koch J., *Arkiv Mat. Astron. Fysik*, **10**, (1914)
[45] Frolich C., G.E. Shaw, New determination of Rayleigh scattering in the terrestrial atmosphere, *J. Opt. Soc. Am.*, **19**, 1773-1775,(1980).
[46] Kerker M., *The Scattering of Light and Other Electromagnetic Radiation*, Academic, N.Y., (1969).
[47] Penndorf R.,Tables of the Refractive Index of air and the Rayleigh Scattering Coefficient for the Spectral Range between 0.2 um and 20 um and Their Application to Atmospheric Optics, *J.Opt.Soc.Am.*,**47**(2),176-182,(1957).
[48] Hoyt D.V., A Redetermination of the Rayleigh Optical Depth and its Application to Selected Solar Radiation Problems, *J.Appl.Meteorol.*,16,432-436,(1977).
[49] Young A.T., Revised depolarisation corrections for Atmospheric Extinction, *Appl.Opt.*, **19**, 3427-3428, (1980)
[50] Bakan,Hinzpeter, Atmospheric radiation
[51] Bates D.R., Rayleigh scattering by air, *Planet.Space Sci.*, **32**, 785, (1984)
[52] Peck E.D.,K.Reeder,*J.Opt.Soc.Am.*,**58**,1260,(1968).
[53] Teillet P.M., Rayleigh optical depth comparisons from various sources, *Appl.Opt.*,**29**(13),1897-1900,(1990).

[54] Edlen B.,The refractive index of air, *Meteorology*, **2**, 71-80,(1966).
[55] Malicet J., D.Daumont, J.Charbonnier, C.Parisse, A.Chakir, J.Brion, Ozone UV Spectroscopy. II. Absorption Cross-Sections and Temperature Dependence, *J.Atm.Chemistry*, **21**, 263-273,(1995).
[56] Yoshino K., D.E.Freeman, J.R.Esmond, W.H.Parkinson, Absolute cross-section measurement of ozone in the wavelength region 238-335 nm and the temperature dependence, *Planet.Space Sci.*, **36**, 395-398,(1988).
[57] Yoshino K., J.R.Esmond, D.E.Freeman, W.H.Parkinson, Measurements of the absolute cross-sections of ozone in the 185 to 254 nm wavelength region and the temperature dependence, *JGR*, **98**, 5205-5211,(1993)
[58] Molina L.T., M.J.Molina, Absolute absorption crossections of ozone in the 185 to 350 nm wavelength range, *JGR*, **91**, 14501-14508, (1986)
[59] Bass A.M., R.J.Paur,*The ultraviolet cross-sections of ozone, I. Measurements*, in C.Zeferos and A.Ghazi (eds.),Proc. Quadrennial Ozone Symp. Halkidiki, Greece, Reidel,Dordrecht,606-616,(1984).
[60] Cacciani M., Di Sarra, G.Fiocco,, A.Amouroso, Absolute determination of the cross sections of ozone in the wavelength regin 339-355 nm at temperatures 220-293 K, *JGR*, **94**, 8485-8490,(1989)
[61] Kirmse B., A.Delon, R.Jost, NO2 absorption crossection and its temperature dependence, *JGR*, **102**, 16089-16098,(1997)
[62] Merienne M.F., A.Jenouvrier, B.Coquart, The NO2 Absorption Spectrum. I: Absorption Cross-Sections at Ambient Temperature in the 300-500 um Region, *J.Atmos.Chem.*, **20**, 281-297, (1995)
[63] Coquart B., A.Jenouvrier, M.F.Merienne, The NO2 absorption spectrum. II. Cross-Sections at Low Temperatures in the 400-500 nm Region, *J.Atmos.Chem.*, **21**, 251-261, (1995)
[64] Jenouvrier A.,B.Coquart, M.F.Merienne, The NO2 absorption spectrum. III. The 200-300 nm Region at Ambient Temperature, *J.Atmos.Chem.*, **25**, 21-32, (1996)
[65] Vandaele A.C., C.Hermans, P.C.Simon,M. VAN Roozendael, J.M.Gulmot, M.Carleer, R.Colin, Fourier Transform Measurements of NO2 Absorption Cross-Sections in the Visible Range at Room Temperature, *J.Atmos.Chem.*, **25**, 289-305, (1996)
[66] Harder J.W., J.W.Brault, P.V.Johnston, G.H.Mount, Temperature dependent NO2 crossections at high spectral resolution, *JGR*, **102**, 3861-3879,(1997)
[67] DeMore W.B., S.P.Sander, D.M.Golden, R.F.Hampson, M.J.Kurylo, C.J.Howard, A.R.Ravishankara, C.E.Kolb, M.J.Molina,*Chemical Kinetics and Photochemical Data for Use*

in Stratospheric Modeling, Evaluation Number 12, JPL Publication 97-4,NASA JPL,CIT,Pasadena, California,(1997).
[68] Davidson J.A., C.A. Cantrell, A.M.McDaniel, R.E.Shetter, S.Madronich, J.G.Calvert, Visible ultraviolet absorption cross-sections of NO2 as a function of temperature, *JGR*, **93**, 7105-7112, (1988)
[69] Schneider W., G.K. Mootgart, G.S.Tyndall, J.P.Burrows, Absorption cross-sections of NO2 in the UV and visible region (200-700 nm) at 298K, *J.Photochem.Photobiol.*, **40**,195-217,(1987).
[70]Burrows J.P, A.Dehn, B. Deters, S. Himmelmann, A. Richter, S. Voigt, J. Orphal, Atmospheric Remote-Sensing Reference Data from GOME: 2. Temperature-Dependent Absorption Cross Sections of O3 in the 231-794 nm range, *JQSRT*, **61**, 509-517, (1999).
[71] Burrows J.P, A.Dehn, B. Deters, S. Himmelmann, A. Richter, S. Voigt, J. Orphal, Atmospheric Remote-Sensing Reference Data from GOME: 1. Temperature-Dependent Absorption Cross Sections of NO2 in the 231-794 nm range, *JQSRT*, **60**, 1025-1031, (1998).
[72] Chang J.S.,Brost R.A.,Isaksen I.S.A.,Madronich S., Middleton P., Stockwell W.R., Walcek C.J., A three dimensional Eulerian acid deposition model: physical concepts and formation, *JGR*, **92**, 14681-14700,(1987)
[73] Stockwell W.R.,Middleton P.,Chang J.S., Tang X., The second generation regional acid deposition model: Chemical mechanisms for regional air quality modelling, *JGR*, **95**, 16343-16367,(1990)
[74] Hoffman R.J., J.M. Rosen, T.J. Pepin, R.G. Pinnick,`Stratospheric Aerosol Measurements I: Time Variations at Northern Latitudes, *JAS*, **32**,1446-1456, (1975).
[75] d'Almeida G.A., On the Variability of Desert Aerosol Radiative Characteristics, *JGR*, **92**, 3017-3026,(1987)
[76] Koepke P., M. Hess, I. Schult, E.P. Shettle, *Global aerosol data set*, Report N243, Max-Planck Institute for Meteorology, Hamburg, Germany,(1997)
[77] Mishchenko M.I., A.A. Lacis, B.E. Carlson, L.D. Travis, Nonsphericity of dust-like tropospheric aerosols: implications for aerosol remote sensing and climate modelling, *Geophys. Res. Lett.*, **22**(9), 1077-1080, (1995).
[78] Kondo Y., T. Sugita, R.J. Salawitch, M. Koike, T. Deshler, Effect of Pinatubo aerosols on stratospheric NO, *JGR*, **102** (D1), 1205-1213, (1997).
[79] Rosenfield J.E., D.B. Considine, P.E. Meade, J.T. Bacmeister, C.H. Jackman, M.R. Schoeberl,Stratospheric effects of Mount Pinatubo aerosol studied with a coupled two-dimensional model, *JGR*, **102**(D3), 3649-3670, (1997).

[80] Huang T.Y.W, S.T. Massie, Effect of volcanic particles on the O2 and O3 photolysis rates and their impact on ozone in the tropical stratosphere, *JGR*,**102** (D1), 1239-1249,(1997)
[81] Stenchikov G.L., I. Kirchner, A.Robock, H.-F. Graf, J.C. Antuna, R. Grainger, A. Lambert, L. Thomason, *JGR*,in press, (1997).
[82] Roeckner E., K. Arpe, L. Bengtsson, M. Christoph, M. Clausse, L. Dumenil, M. Esch, M. Giorgetta, U. Schlese, U. Schulzweida, *The atmospheric general circulation model ECHAM-4: Model description and simulation of the present climate,* Report of the Max-Planck Institute for Meteorology, N 218, MPIfM, Hamburg, (1996)
[83] Jacob D., Podzun R., *Meteorology and Atmospheric Physics,* **63**(1), 119,(1990).
[84] Johnson, *Parameterisation of the cloud topped boundary layer,* in ECMWF Workshop Proceedings, 77-117,Reading, UK, (1993).
[85] McFarlane, Boer, Blanchet, Lazare, The Canadian Climate Centre second-generation general circulation model and its equilibrium climate, *J.Climate*, **5**, 1013-1044,(1992).
[86] Hu Y.X., K. Stamnes, An accurate parameterisation of the radiative properties of water clouds suitable for use in the climate models, *J. Climate*, **6**(4), 728-742, (1993).
[87] Hass H., A. Ruggaber, *Meteorol. Atmos. Phys.*, **57**, 87-100, (1995).
[88] Gabriel P.M, K.F. Evans, Simple Radiative Transfer Methods for Calculating Domain-Averaged Solar Fluxes in Inhomogeneous Clouds, *J. of Atmos. Sci.*, **53**, 858-877, (1996).
[89] Ritter B., *Radiative transfer simulation in NWP models of high horisontal resolution: the inadequacy of 1-dimensional approach,* in the proceedings of IRS'96:Current Problems in Atmospheric Radiation, Smith and Stamnes (eds.), A.Deepak, (1997).
[90] Ackerman T., M.B. Baker, Shortwave Radiative Effects of Unactivated Aerosol Particles in Clouds, *J. of Appl. Meteorol.*, **16**, 63-69,(1997)
[91] Svenningson B., H.-C. Hansson,A. Wiedensohler, K. Noone, J. Ogren, A. Hallberg, R. Colvile, Hygroscopic Growth of Aerosol Particles and its Influence on Nucleation Scavenging in Cloud: Experimental Results from Kleiner Feldberg, *J. Atmos. Chem*, **19**, 129-152, (1994)
[92] Hallberg A., K.J. Noone, J.A. Ogren, I.B. Svenningsson, A. Flossmann, A. Wiedensohler, H.-C. Hansson, J. Heintzenberg, T.L. Anderson, B.G. Arends,R.Maser, Phase Partitioning of Aerosol Particles in Clouds at Kleiner Feldberg, *J. Atmos. Chem*, **19**, 107-127, (1994)

[93] *Kleiner Feldberg Cloud-Aerosol Experiment*, Special Issue of the *J. Atmos. Chem*, **19**, (1994)
[94]Svenningson B., H.-C. Hansson,A. Wiedensohler, K. Noone, J. Ogren, A. Hallberg, Hygroscopic growth of the aerosol particles in the Po Valley, *Tellus*, **44B**, 556-569, (1992).
[95] Noone K.J, J.A. Ogren, A. Hallberg, J. Heintzenberg, J. Strom, J. Hansson, H.-C. Svenningson, S. Fuzzi, M.C. Facchini, A. Wiedensohler, B.G. Arends, A. Berner, Changes in aerosol size- and phase distributions due to physical and chemical processes in for, *Tellus*, **44B**, 489-504, (1992)
[96] Macke A., M.I. Mishchenko, B. Cairns, *The influence of inclusions on light scattering by large hexagonal and spherical ice crystals*, in the proceedings of IRS'96:Current Problems in Atmospheric Radiation, Smith and Stamnes (eds.), A.Deepak, (1997).
[97] Bowker D.E., R.E. Davis, D.L. Myrick, K. Stacy, W.T. Jones, *Spectral reflectances of natural targets for use in remote sensing studies*, NASA Ref. Publ. 1139, (1985).
[98] Eaton F.D., Dirmhirn I., *Appl. Opt.*, **18**, 944, (1979).
[99] Tanre et al, *Simulation of the satellite signal in the solar spectrum (5S)*, Laboratoire d'Optique Atmospherique, 262 pp, (1986).
[100] McLinden C.A., D.J. Chartrand, E. Griffioen, J.C. McConnell, C.T. McElroy, The Impact of Non-Lambertian Wavelength-Dependent Reflecting Surfaces on Stratospheric Radiation and Photochemistry, *J. of Atmos. Chem.*, **26**, 29-64, (1997).
[101] Capderou M., *Determination of the shortwave anisotropic function for clear sky desert scenes from SCARAB data*, in the proceedings of IRS'96:Current Problems in Atmospheric Radiation, Smith and Stamnes (eds.), A.Deepak, (1997).
[102] Gardner E.P., P.D. Sperry, J.G. Calvert, Primary Quantum Yields of NO2 Photodissociation, *JGR*, **92**(D6),6642-6654, (1987).
[103] Michelsen H.A.,R.J.Salawitch, P.O. Wennberg, J.G. Anderson, Production of O(1D) from photolysis of O3, *Geophys. Res. Lett.*, **21**(20), 2257-2230, (1994).
[104] Muller M., A. Kraus, A. Hofzumahaus, O3->O(1D) photolysis frequences determined from spectroradiometric measurements of solar actinic UV-radiation: Comparison with chemical actinometer measurements, *Geophys. Res. Lett.*, **22**(6), 679-682, (1995).
[105] Ball S.M., G Hancock, The relative quantum yields of O2(a1<delta>g) from the photolysis of ozone at 227K, *Geophys. Res. Lett.*, **22**(10), 1213-1216, (1995).
[106] Christensen J.H., O.B. Christensen, P. Lopez, E.V. Neijgaard, N. Botzet, *The HIRHAM regional atmospheric*

climate model, Scientific Report 96-4, Danish Meteorological Institute, Copenhagen , Danemark, (1996)
[107] Dickerson R.R., D.H. Stedman, A.C. Delany, Direct Measurements of Ozone and Nitrogen Dioxide Photolysis Rates in the Troposphere, *JGR*, **87**(C7), 4933-4946, (1982).
[108] Parrish D.D., P.C. Murphy, D.L. Albritton, F.C. Fehsenfeld, The measurement of the photodissociation rate of NO2 in the atmosphere, *Atmos. Environ.*, **17**(7),1365-1379, (1983).
[109] Jaegle L., C.R. Webster, R.D. May, D.W. Fahey, E.L. Woodbridge, E.R. Keim, R.S. Gao, M.H. Proffitt, R.M. Stimpfle, R.J. Salawitch, S.C. Wofsy, L. Pfister, In situ measurements of the NO2/NO ratio for testing atmospheric photochemical models, *Geophys. Res. Lett.*, **21**(23), 2555-2558, (1994).
[110] Feister U., Measurements of Chemically and Biologically Effective Radiation Reaching the Ground, *J. of Atmos. Chem.*, **19**, 289-315, (1994).
[111] McElroy C.T., C. Midwinter, D.V. Barton, R.B. Hall, A comparison of J-values from the composition and photodissociative flux measurement with model calculations, *Geophys. Res. Lett.*, **22**(10), 1365-1368, (1995).
[112] Kelley P., R.R. Dickerson, W.T. Luke, G.L. Kok, Rate of NO2 photolysis from the surface to 7.6 km altitude in clear-sky and clouds, *Geophys. Res. Lett.*, **22**19), 2621-2624, (1995).
[113] Dickerson R.R., S. Kondragunta, G. Stenchikov, K.L. Civerolo, B.G. Doddridge, B. Holben, The Impact of Aerosols on Solar UV Radiation and Photochemical Smog, *Science*, accepted, (1997).
[114] Blindauer C., V. Rozanov, J.P. Burrows, Actinic Flux and Photolysis Frequency Comparison Computations Using the Model PHOTOGT, *J. of Atmos, Chem.*, **21**, 1-21, (1996).
[115] Langmann B., H.-F.Graf, *Atmos. Environ*, **31**(9), 3239-3257,(1997).
[116]de F. Forster, Piers M., Modelling Ultraviolet Radiation at the Earth's Surface. Part I: The Sensitivity of Ultraviolet Irradiances to Atmospheric Change, *J. of Apll. Meteorol.*, **34**, 2412-2425, (1995).
[117]Weihs P., A.R. Webb, Accuracy of spectral UV model calculations.1. Consideration of uncertainties in input parameters, *JGR*, **102**(D1), 1541-1550, (1997).
[118] Weihs P., A.R. Webb, Accuracy of spectral UV model calculations. 2. Comparison of UV calculations with measurements, *JGR*, **102**(D1), 1551-1560, (1997).
[119] Schwander H., P. Koepke, A. Ruggaber, *Uncertainties in the modeled UV-irradiances due to limited accuracy and availability of input data*, in the proceedings of

IRS'96:Current Problems in Atmospheric Radiation, Smith and Stamnes (eds.), A.Deepak, (1997).

[120] de F. Forster, Piers M., K.P. Shine, A.R. Webb, Modelling Ultraviolet Radiation at the Earth's Surface. Part II: Model and Instrument Comparison, *J. of Apll. Meteorol.*, **34**, 2426-2439, (1995).

[121] Barichello L.B., R.D.M. Garcia, C.E. Siewert, The Fourier decomposition for a radiative-transfer problem with an asymmetrically reflecting ground, *JQSRT*,**56**(3),363-371, (1996).

[122] Godsalve C., The inclusion of reflectances with preferred directions in radiative transfer calculations, *JQSRT*, **56**(3), 373-376, (1996).

[123] Settle J.J, Some exact solutions for coupled atmosphere-surface radiation models, *JQSRT*, **56**(1), 47-55, (1996).

[124] Leroux C., J. Lenoble, J.L. Deuze, P. Goloub, *Modelling and measurement of snow reflectance from visible to near infrared*, in the proceedings of IRS'96:Current Problems in Atmospheric Radiation, Smith and Stamnes (eds.), A.Deepak, (1997).

[125] Steffen K., *Effect of solar zenith angle on snow anisotropic reflectance*, in the proceedings of IRS'96:Current Problems in Atmospheric Radiation, Smith and Stamnes (eds.), A.Deepak, (1997).

[126] Aoki T., T. Aoki, M. Fukabori, *Effects of the different types of the atmospheres on the surface and planetary albedos of snow*, in the proceedings of IRS'96:Current Problems in Atmospheric Radiation, Smith and Stamnes (eds.), A.Deepak, (1997).

[127] Elbern H., H. Schmidt, A. Ebel, Variational data assimilation for tropospheric chemistry modelling, *J. of Geophys. Res.*, **102**(D13), 15967-15985, (1997).